IgH isotype-specific B cell receptor expression influences B cell fate

Pei Tong[a,1], Alessandra Granato[a,1], Teng Zuo[a], Neha Chaudhary[a], Adam Zuiani[a], Seung Seok Han[a], Rakesh Donthula[a], Akritee Shrestha[a], Debattama Sen[a], Jennifer M. Magee[a], Michael P. Gallagher[a], Cees E. van der Poel[b,c], Michael C. Carroll[b,c], and Duane R. Wesemann[a,2]

[a]Division of Rheumatology, Immunology and Allergy, Brigham and Women's Hospital, and Department of Medicine, Harvard Medical School, Boston, MA 02115; [b]Program in Cellular and Molecular Medicine, Children's Hospital Boston, Harvard Medical School, Boston, MA 02115; and [c]Department of Pediatrics, Harvard Medical School, Boston, MA 02115

Edited by Klaus Rajewsky, Max Delbrück Center for Molecular Medicine, Berlin, Germany, and approved August 16, 2017 (received for review March 28, 2017)

Ig heavy chain (IgH) isotypes (e.g., IgM, IgG, and IgE) are generated as secreted/soluble antibodies (sIg) or as membrane-bound (mIg) B cell receptors (BCRs) through alternative RNA splicing. IgH isotype dictates soluble antibody function, but how mIg isotype influences B cell behavior is not well defined. We examined IgH isotype-specific BCR function by analyzing naturally switched B cells from wild-type mice, as well as by engineering polyclonal *Igh*γ1/γ1 and *Igh*ε/ε mice, which initially produce IgG1 or IgE from their respective native genomic configurations. We found that B cells from wild-type mice, as well as *Igh*γ1/γ1 and *Igh*ε/ε mice, produce transcripts that generate IgM, IgG1, and IgE in an alternative splice form bias hierarchy, regardless of cell stage. In this regard, we found that mIgμ > mIgγ1 > mIgε, and that these BCR expression differences influence respective developmental fitness. Restrained B cell development from *Igh*γ1/γ1 and *Igh*ε/ε mice was proportional to sIg/mIg ratios and was rescued by enforced expression of the respective mIgs. In addition, artificially enhancing BCR signal strength permitted IgE$^+$ memory B cells—which essentially do not exist under normal conditions—to provide long-lived memory function, suggesting that quantitative BCR signal weakness contributes to restraint of IgE B cell responses. Our results indicate that IgH isotype-specific mIg/BCR dosage may play a larger role in B cell fate than previously anticipated.

B cell | antibody | IgE | BCR | memory

Ig heavy chain (*IgH*) constant region (C_H) isotypes enable coupling of antigen-binding *Ig* variable regions (V) to diverse functional contexts. The C_H exons are arranged in tandem, with Cμ (encoding the IgM constant region) initially located most proximal to the *Ig* V_H exon, followed by a number of alternative C_H isotypes (e.g., Cγ, Cε, and Cα). Each C_H is supplied with terminal exon(s) encoding transmembrane and cytoplasmic tail moieties enabling expression of membrane Ig (mIg), which, together with the CD79A and CD79B signaling accessory proteins, form the antigen-binding part of the B cell receptor (BCR) (1). Mutually exclusive alternative splicing can exclude membrane exons to produce secreted Ig (sIg) (2).

Ig V exons of IgH and Ig light (IgL) chains are assembled in bone marrow (BM) progenitor (pro) and precursor (pre) B cells, respectively (3). Productive V_H and V_L assembly results in IgM expression on the surface of immature B cells, which further develop to mature naïve IgM$^+$ IgD$^+$ B cells upon emigration from the BM to the periphery, where they can participate in immune responses. Activated B cells can undergo *Igh* class switch recombination (CSR), mediated by activation-induced cytidine deaminase (AID). CSR replaces initially expressed IgM with IgG, IgE, or IgA by targeted repositioning of the alternative *Igh* locus C_Hs, resulting in permanent deletion of intervening C_Hs (4). Following activation, B cells can maintain a general B cell transcriptional program to support the production of long-lived memory B cells, which continue to be dependent upon BCR signals. An alternate fate results from a large shift in the general B cell transcriptional program toward specialization as antibody secreting cells (ASCs) (5).

IgH CSR is associated with different IgH isotype-specific B cell fates following activation (6–12). Investigations into mechanisms underlying how IgH isotype influences BCR/mIg function to date have largely relied upon overexpression and transgenic experiments of monoclonal Ig to identify how differences in protein sequence between IgH isotypes influence BCR signaling (13–18). However, whether differences of endogenous BCR expression from the *Igh* locus occur between isotypes is not fully defined. To address this, we generated preswitched *Igh*ε/ε and *Igh*γ1/γ1 mice engineered to produce polyclonal IgE and IgG1 B cells, respectively, to explore the role of IgH isotype on BCR function from native genomic contexts. We identified an isotype-specific BCR expression hierarchy in naïve IgG1 and IgE B cells from preswitched mice that is preserved in B cells after regular activation-induced CSR. We report that *Igh* isotype-specific BCR expression is an underlying feature that contributes to isotype-specific B cell behaviors.

Results

Generation of *Igh*ε/ε and *Igh*γ1/γ1 Mice. To explore the degree to which IgH isotype regulates BCR function, we generated *Igh*ε/ε

Significance

B cells produce antibodies in the context of immunoglobulin heavy chain (IgH) isotypes (e.g., IgM, IgG, and IgE). Each of these is generated either as secreted proteins or as membrane-bound B cell antigen receptors (BCRs). While much is known about how IgH isotype dictates effector function of soluble antibodies, the role of antibody isotype in the context of BCRs is not well defined. Here we demonstrate that the membrane-bound versions (mIg) of IgM, IgG1, and IgE are produced from their natural genomic loci in a hierarchal fashion, where mRNA transcripts for mIgM are always more dominant than mIgG1, which are always more dominant than mIgE, regardless of cell stage. These isotype-specific expression differences contribute to B cell regulation.

Author contributions: P.T., A.G., T.Z., and D.R.W. designed research; P.T., A.G., T.Z., A.Z., S.S.H., R.D., A.S., D.S., J.M.M., and M.P.G. performed research; C.E.v.d.P. and M.C.C. contributed new reagents/analytic tools; P.T., A.G., T.Z., N.C., A.Z., S.S.H., D.S., and D.R.W. analyzed data; P.T., A.G., and D.R.W. wrote the paper; and D.R.W. conceptualized the study.

The authors declare no conflict of interest.

This article is a PNAS Direct Submission.

Data deposition: The raw sequence data for this study are accessible at the NCBI Sequence Read Archive (SRA) under BioProject accession no. PRJNA394007 with BioSample accession nos. SAMN07347175–SAMN07347206.

[1]P.T. and A.G. contributed equally to this work.

[2]To whom correspondence should be addressed. Email: dwesemann@bwh.harvard.edu.

This article contains supporting information online at www.pnas.org/lookup/suppl/doi:10.1073/pnas.1704962114/-/DCSupplemental.

and *Igh*γ1/γ1 mice in an effort to produce native polyclonal IgE$^+$ and IgG1$^+$ B cells, respectively, from natural genomic contexts. The *Igh*ε/ε mice were derived from induced pluripotent stem cells (iPSCs) generated from B-lineage cells that had previously undergone IgH CSR to IgE on an allele that had rearranged a D_H to J_H1, but that had not yet undergone V_H to D_HJ_H assembly (Fig. 1*A* and *SI Appendix*, Fig. S1*A*). The *Igh*γ1/γ1 mice were generated by deletion of a portion of the C_H locus such that the resulting arrangement would be identical to a natural CSR event to *Cγ1*. This was achieved by CRISPR-mediated embryonic stem cell (ESC) targeting of the same DNA regions targeted for DNA cleavage events during CSR from *C*μ to *Cγ1* (Fig. 1*A* and *SI Appendix*, Fig. S1*B*).

Differential B-Lineage Developmental Competence in *Igh*ε/ε and *Igh*γ1/γ1 Mice. Early B cell maturation requires BCR signals to license maturation through developmental stages. Productive assembly of *Ig*μ in the pro–B cell stage leads to surface assembly of the pre-BCR, containing mIgμ, a surrogate light chain complex (SLC), and the CD79A/B proteins. Pre-BCR signaling stimulates *Igl* (*Ig*κ or *Igl*λ) *V* exon assembly in pre-B cells. Productively assembled *Igl* produces Igκ or Iglλ, which complexes with mIgμ to form IgM, which together with CD79A/B, form the BCR on the surface of immature B cells that provided signals for continued B cell development (19).

We examined the competence of IgE and IgG1 as BCRs to support BCR-dependent developmental steps during early B-lineage cell maturation. We found that *Igh*ε/ε mouse BM contains abundant B220^{lo} CD43$^+$ pro-B cells; however, CD43$^-$ B220^{int} pre-B, BCR$^+$ immature, and B220^{hi} BCR$^+$ recirculating B cells, were severely reduced in amount (Fig. 1*B*). In addition, IgE$^+$ B cells in the spleen were nearly undetectable (Fig. 1 *C* and *D*). Developmental blockade in *Igh*γ1/γ1 mice was not as severe, with detectable BM immature and recirculating B cells (Fig. 1*B*) and a clear splenic B cell population numbering over 10-fold less compared with wild-type and heterozygous mice (Fig. 1 *C*–*E*). BM pro-B cells from each mouse expressed levels of IL-7 receptor similar

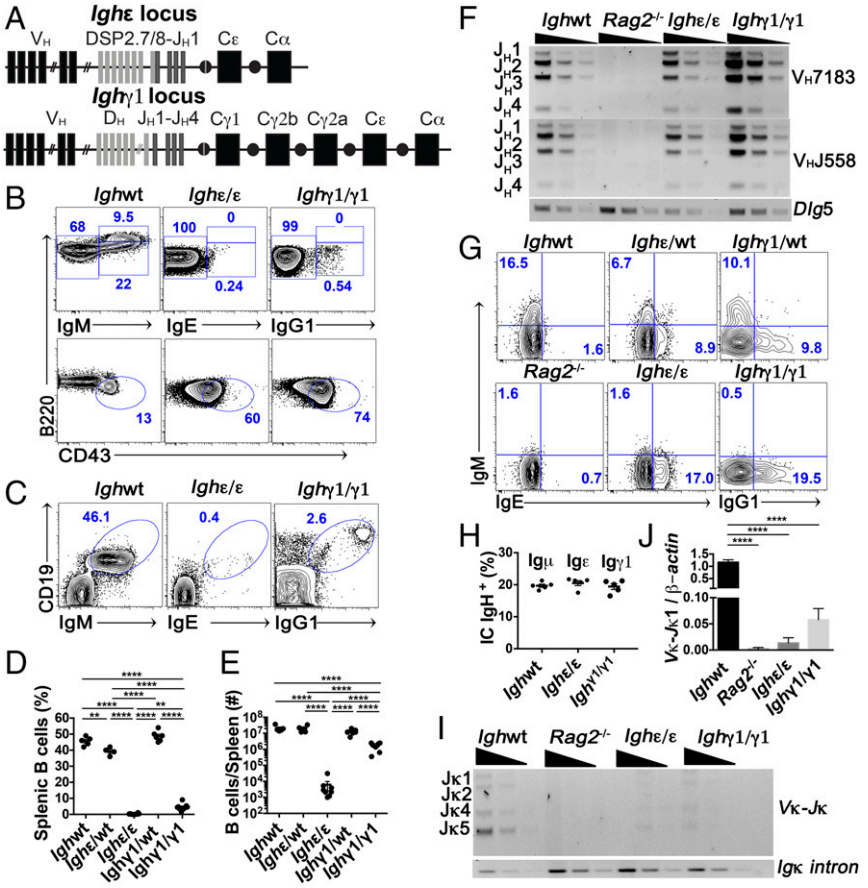

Fig. 1. B cell development in *Igh*ε/ε and *Igh*γ1/γ1 mice is impaired. (*A*) Schematic representations of the *Igh*ε (*Top*) and *Igh*γ1 (*Bottom*) alleles. (*B*) FACS plots of live CD19$^+$ and B220$^+$ bone marrow cells (*Top* plots) as well as live B220$^+$ CD19$^+$ and BCR$^-$ (*Bottom* plots). Mature recirculating B cells (B220^{hi} BCR$^+$), immature B cells (B220^{int} BCR$^+$), and pro–B cell (B220^{lo} BCR$^-$ CD43$^+$) frequencies are indicated ($n = 6$). (*C*) FACS plots of splenic lymphocytes showing CD19 expression versus IgM, IgE, or IgG1 from the indicated mice ($n = 6$). (*D* and *E*) Dot graph showing summary statistics of percentages (*D*), and total number (*E*), of splenic B cells from the indicated mice. Each dot represents one mouse ($n = 4$–9). (*F*) Semiquantitative PCR analyses of J_H-proximal V_H7183 and J_H-distal V_HJ558 family rearrangements in sorted bone marrow pro-B cells from indicated mice. Dlg5 was amplified as a loading control. Threefold serial dilutions are shown. Results are typical of three experiments. Bands corresponding to rearrangements to various J_H segments are indicated. (*G*) FACS plots showing intracellular Igμ, Igε, and Igγ1 heavy chain in pro-B cells (CD19$^+$ B220^{lo} Igκ$^-$ CD43$^+$) from bone marrows of the indicated mice. Results are typical of at least four experiments. (*H*) Percentage of intracellular Igμ, Igε, and Igγ1 heavy chain in BM pro-B cells. Each dot represents one mouse ($n = 5$). (*I*) Semiquantitative PCR analyses of *Vκ Igl* chain rearrangements in magnetically separated bone marrow B220$^+$ cells from indicated mice. Intronic *Ig*κ was amplified as a loading control. Threefold serial dilutions are shown. Bands corresponding to rearrangements to various *Jκ* segments are indicated on the *Left*. Results are typical of four experiments. (*J*) Quantitative PCR analyses of *Vκ* to *Jκ*1 *Igl* chain rearrangement relative to β-*actin* DNA in purified B220$^+$ BM cells from the indicated mice. Expression is shown as fold change relative to wild-type levels. $^{**}P < 0.01$, $^{****}P < 0.0001$; one-way ANOVA followed by Tukey's post hoc test. Summary data are mean values ± SEM. See also *SI Appendix*, Figs. S1 and S2.

to wild type (*SI Appendix*, Fig. S2*A*) and both had a similar mild reduction of proliferation capacities when stimulated ex vivo with low doses of IL-7, although this did not reach statistical significance (*SI Appendix*, Fig. S2*B*). These data suggest that endogenously produced, polyclonal IgE and IgG1 have different levels of BCR fitness in a model of early B cell development, with IgE being the most severely restricted.

Igγ1 and Igε Proteins Are Produced in Pro-B Cells, but Provide Insufficient Stimuli to Induce *Igκ* Assembly. To determine whether blockade of B cell development is due to inhibition of VDJ_H recombination, we assessed the level of *Igh* VDJ_H recombination of the two main V_H families (proximally positioned 7183, and distally positioned J558 families) on sorted BM B cell progenitors by semiquantitative PCR. *Igh*ε/ε and *Igh*γ1/γ1 mice showed similar levels of assembled VDJ_H compared with wild-type progenitor B cells (Fig. 1*F*). Despite the preassembled D_H to J_H1 assembly in *Igh*ε/ε mice, all J_Hs were used (Fig. 1*F*). In addition, flow cytometric analysis of intracytoplasmic IgH expression in pro-B cells demonstrated similar levels of intracellular Igε and Igγ1 compared with wild-type pro-B cells expressing Igμ (Fig. 1 *G* and *H*). In addition, heterozygous *Igh*ε/*WT*, as well as *Igh*γ1/*WT* heterozygote B cell progenitors show Igε:Igμ and Igγ1:Igμ ratios of 1:1 for each (Fig. 1 *G* and *H* and *SI Appendix*, Fig. S2 *C* and *D*). These data demonstrate both Igε and Igγ1 heavy chains are expressed intracytoplasmically at levels very comparable to Igμ. Despite this, mature B cells from both *Igh*ε/*WT* and *Igh*γ1/*WT* mice are essentially all IgM^+, suggesting a strong competitive advantage for Igμ over Igγ1 or Igε in later stages of development.

To determine the degree to which allelic exclusion is affected, we performed quantitative analysis of cells expressing both *Igh* alleles in *Igh*ε/*WT* and *Igh*γ1/*WT* heterozygous mice from developing BM and splenic B cells. While intact allelic exclusion makes IgH production from both alleles scarce (less than 1%), a full break in allelic exclusion would theoretically be indicated by 12.2% of double producers (20), although in practice this may be less due to the ability of IgH mRNA from productively assembled *Igh* loci to mediate allelic exclusion of homologous loci in the absence of IgH protein (21). Within the pool of IgH-expressing $B220^{lo}$ $CD43^+$ BM B-lineage cells, we found 5–8% double IgH producers in both *Igh*ε/*WT* and *Igh*γ1/*WT* heterozygous mice (*SI Appendix*, Fig. S2 *C* and *D*). For splenic B cells, 2–3% express both IgM and IgG1 in *Igh*γ1/*WT* mice, whereas 5–7% are positive for both IgM and IgE in *Igh*ε/*WT* mice (*SI Appendix*, Fig. S2 *E* and *F*). Of note, cells heterozygous for an allele that can only produce the secreted version of IgM (μMT allele) (22), also contain ∼6% of double producers in the spleen (20). This analysis suggests that IgG1, and to a greater extent, IgE, are unable to mediate normal allelic exclusion.

To determine the degree of *Igl* rearrangement in *Igh*ε/*WT* and *Igh*γ1/*WT* mice, we assessed *Igκ V-J* rearrangement by semiquantitative PCR as well as the level of rearrangement to *J*κ1 by qPCR. We found that *Igh*ε/ε BM B cell *Igκ* rearrangement is very near the *Rag2*$^{-/-}$ background control with *Igh*γ1/γ1 *Igκ* rearrangement slightly higher (Fig. 1 *I* and *J*). Together, these results indicate that, while IgH intracytoplasmic expression reaches wild-type Igμ levels, BCR signaling in the context of endogenously produced Igγ1 and Igε provides insufficient signaling to stimulate entry into subsequent BCR-dependent cell stages.

***Igh*γ1/γ1 and *Igh*ε/ε B Cell Development Is Partially Rescued by a Pre-Assembled *Igκ* (*VJκ5*).** To determine the extent to which introduction of a preassembled *Igκ* can rescue development in *Igh*γ1/γ1 and *Igh*ε/ε B cells, we crossed both *Igh*γ1/γ1 and *Igh*ε/ε mice to the *VJ*κ5 allele, a natural productive *Igκ* assemblage, also produced via B cell to iPSC reprogramming (*SI Appendix*, Fig. S1*C*). The presence of the preassembled *VJ*κ5 resulted in a partial rescue of the developmental blockade observed in *Igh*ε/ε mice. IgE^+ B cells in *Igh*ε/ε*VJ*κ5 mice increased in percentage (Fig. 2 *A* and *B*), with an ∼10-fold increase in splenic B cell number (compare Fig. 1*E* to Fig. 2*C*). $IgG1^+$ cells increased ∼5-fold in *Igh*γ1/γ1 mice (compare Fig. 1*E* to Fig. 2*C*). We found that mature IgE^+ B cells from *Igh*ε/ε*VJ*κ5 mice are nearly all of the follicular B cell phenotype ($CD19^+$ $B220^+$ $CD93^-$ $CD23^{hi}$ $CD21^{int}$), whereas splenic $IgG1^+$ cells from *Igh*γ1/γ1 and *Igh*γ1/γ1*VJ*κ5 mice have both follicular and marginal zone ($CD19^+$ $B220^+$ $CD93^-$ $CD23^{lo}$ $CD21^{hi}$) populations in the splenic B cell compartment, with an increased percentage of marginal zone B cells compared with wild-type mice (Fig. 2*D*). The $CD19^+$ $IgG1^-$ cells observed in *Igh*γ1/γ1 mice spleens (Fig. 1*C*) expressed CD43 and CD93, consistent with pro-B cells (*SI Appendix*, Fig. S3*A*). In addition, despite significant B lymphopenia, *Igh*ε/ε mice and *Igh*ε/ε*VJ*κ5 mice have 100- to 1,000-fold higher serum IgE levels (Fig. 2*E*) compared with wild-type controls. IgG1 levels in both *Igh*γ1/γ1 and *Igh*γ1/γ1*VJ*κ5 mice are ∼10-fold higher than wild type (Fig. 2*F*).

Analysis of BM and transitional cell populations demonstrated that the *VJ*κ5 allele had a large effect increasing the BM populations for *Igh*γ1/γ1*VJ*κ5 mice, particularly immature B cells (*SI Appendix*, Fig. S3 *B–F*), whereas in *Igh*ε/ε*VJ*κ5 mice, the largest effect appeared to be an increase in $CD93^+$ transitional B cells (*SI Appendix*, Fig. S3 *G–I*). A 26-d pulse of BrdU in drinking water followed by over a month of normal water (chase) showed that the *VJ*κ5 rescue had no significant effect on the maintenance of the circulating B cell pool from *IghWT*, *Igh*ε/ε, and *Igh*γ1/γ1 mice, but did show that both *Igh*ε/ε and *Igh*ε/ε*VJ*κ5 B cells had shorter half lives than the others by about a week (*SI Appendix*, Fig. S4*A*). Together, these data indicate that the developmental arrest in *Igh*γ1/γ1 and *Igh*ε/ε mice can be partially rescued by a preassembled *Igl*, but that the amount of $IgG1^+$ and IgE^+ B cell levels continue to be moderately and severely restricted, respectively, in the periphery, despite both having productive IgH and IgL expression. Enhanced peripheral B cell numbers with preassembled *Igl* also suggests that, in general, BCR signal weakness, rather than too much signal strength, contributes to the developmental blockade in *Igh*γ1/γ1 and *Igh*ε/ε mice.

Mature Naïve IgE^+ and $IgG1^+$ B Cells from *Igh*ε/ε*VJ*κ5 and *Igh*γ1/γ1*VJ*κ5 Mice, Respectively, Are Transcriptionally Similar to Mature Naïve IgM^+ B Cells. We considered the possibility that IgG1 and IgE may direct a plasma cell fate by autonomous signaling (9, 11, 12, 15, 16). To address this, we sorted IgM^+ follicular B cells from wild-type mice and IgE^+ and $IgG1^+$ cells with the same surface phenotype from *Igh*ε/ε*VJ*κ5 and *Igh*γ1/γ1*VJ*κ5 mice, respectively (*SI Appendix*, Fig. S4*B*), to measure gene expression profiles. We found that both IgG1 and IgE B cells align closely to IgM-expressing follicular B cells, with *r* values of 0.975 and 0.946, respectively (Fig. 2 *G* and *H*). We find no differences in genes important for plasma cell differentiation (23) or in core B cell regulatory genes and splicing regulators between IgM, IgE, and IgG1 cells (Fig. 2 *G* and *H*). These data indicate that expression of polyclonal IgG1 and IgE from native loci is not sufficient to directly instruct B cells to become plasma cells when expressed from endogenous genomic context.

IgE and IgG1 B Cells Express Low Cell Surface BCR Density. Previous reports have indicated that BCR density influences B cell fate (8, 24–27). In addition, limited BCR density has been proposed to underlie restriction of IgE B cell numbers (8, 27). To explore the mechanism for the differential insufficiencies of endogenously produced, polyclonal IgG1 and IgE in supporting early B cell development and peripheral B cell numbers, we hypothesized that different BCR dosages may play a role in differential IgG1 and IgE B cell behaviors.

To test this, we measured BCR density by cytometrically assessing Igκ expression on the cell surface of IgM-expressing B cells from wild-type mice and compared them to $IgG1^+$ and IgE^+ B cells from *Igh*γ1/γ1*VJ*κ5 and *Igh*ε/ε*VJ*κ5 mice, respectively.

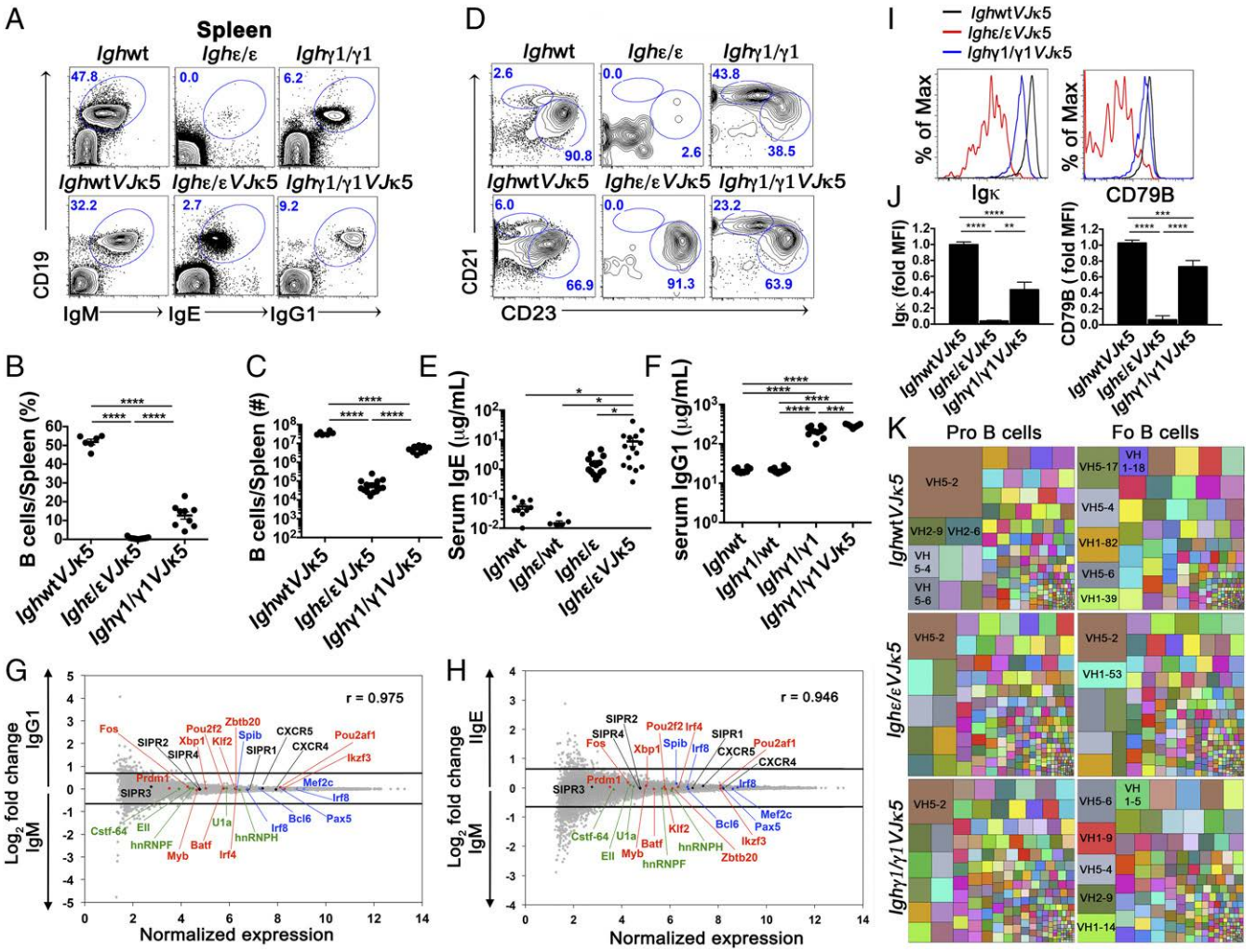

Fig. 2. Development and characteristics of IgE$^+$ and IgG1$^+$ mature B cells with the introduction of a prerearranged *Igκ* (*VJκ*5). (*A*) FACS plots show splenic lymphocytes of the indicated mice. Numbers in the plots indicate percentage of gated live CD19$^+$ BCR$^+$ cells ($n = 6$). (*B* and *C*) Dot graphs showing percentage (*B*) and absolute number (*C*) of splenic B cells of indicated mice. (*D*) FACS plots of live CD19$^+$ B220$^+$ CD93$^-$ gated lymphocytes from spleens of the indicated mice to identify splenic marginal zone (CD21^{hi} CD23^{lo}) and follicular (CD21^{int} CD23^{hi}) B cells ($n = 6$). Because *Ighε/εVJκ5* and *Ighγ1/γ1VJκ5* mice appear to express higher levels of CD23, the gating is relative within each mouse to identify CD23^{hi} CD21^{int} follicular B cells. Numbers in the plots indicate percentages. (*E* and *F*) Total serum IgE (*E*) and IgG1 (*F*) concentration measured by ELISA from the indicated mice. Each dot represents individual mice. (*G* and *H*) Naïve splenic IgE$^+$ and IgG1$^+$ B cells show similar gene expression pattern to WT naïve IgM B cells. Microarray analysis of sorted B220$^+$ CD93$^-$ CD23^{hi} CD21^{int} (follicular) splenic B cells from *IghWTVJκ5* (IgM) versus *Ighγ1/γ1VJκ5* (IgG1) mice (*G*), and *IghWTVJκ5* (IgM) versus *Ighε/εVJκ5* (IgE) mice (*H*). Selected chemokine receptor genes (black), splicing factors (green), as well as positive (red) and negative (blue) regulators of plasma cell differentiation are shown. Lines represent cutoffs for genes up- or down-regulated by a fold-change of at least 0.67 ($\log_2$). The Pearson correlation coefficient (*r*) between gene expression levels is given for respective plots ($n = 3$). (*I* and *J*) Flow cytometric histogram plots (*I*) and summary bar graphs (*J*) of live BCR$^+$ follicular B cells from the indicated mice analyzed for surface Igκ expression (*Left* of *I* and *J*) and CD79B expression (*Right* of *I* and *J*). Fold median fluorescence intensity (MFI) was calculated by dividing MFI values by the average MFI from IgM$^+$ from *IghWTVJκ5* mice for each given subset ($n = 4$–5). *$P < 0.05$, **$P < 0.01$, ***$P < 0.001$, ****$P < 0.0001$; one-way ANOVA followed by Tukey's post hoc test. Data are mean values ± SEM. (*K*) Treemaps showing V_H gene segment frequencies in pro- and follicular (Fo) B cells from *IghWTVJκ5*, *Ighε/εVJκ5*, and *Ighγ1/γ1VJκ5* mice. Each block represents combined data from all biologic repeats ($n = 5$–6). Within a block, each colored box represents one V_H segment. The size of the box is directly proportional to the percentage of sequences, which belongs to the V_H segment. The same V_H segment has the same color in all of the treemaps and the largest boxes contain the V_H name. PCR repeats were removed via unique molecular indexing. See also *SI Appendix*, Figs. S3–S6.

Because the *Ighε/εVJκ5* mice only make B cells with the follicular phenotype, we compared the IgE$^+$ follicular B cells to IgG1$^+$ and IgM$^+$ follicular B cells from the other mice. We also assessed BCR density by staining cells for CD79B (also known as Igβ), as this forms a part of the BCR for all IgH isotypes (28). We found that both Igκ as well as CD79B median fluorescence intensity (MFI) was highest for IgM-expressing naïve follicular B cells, and lowest in IgE$^+$ cells, with IgG1-expressing B cells falling in between the two (Fig. 2 *I* and *J*). These data suggest that BCR dosage may influence B cell numbers by regulating integrated BCR signaling strength.

BCR-Related Phosphoprotein Analysis in IgM, IgG1, and IgE Cells. We also examined baseline phosphorylation levels of Erk, Syk, and Akt, which are related to BCR signaling (29), by flow cytometry. We found that basal phosphorylation levels of Akt were similar, whereas phospho (p)-Erk, and p-Syk were modestly higher in splenic cells from *Ighγ1/γ1VJκ5* and *Ighε/εVJκ5* mice compared with *IghWTVJκ5* mice (*SI Appendix*, Fig. S4*C*). These results are consistent with the concept that intrinsic BCR signaling differences exist between IgH isotypes and may be playing a role in the phenotypic differences. However, the degree to which the phenotypic differences are directly related to the BCR is not clear. Also unclear

is whether or not these differences are a cause or an effect of the developmental blockade.

Given the BCR density differences between IgM, IgG1, and IgE, we assessed levels of BCR-related phosphoproteins in a system where expression levels of BCR isotypes from endogenous loci are similar to each other. For this we generated CH12 cell lines expressing IgM, IgG1, or IgE from endogenous loci (*SI Appendix*, Fig. S4*D*). We find similar levels of baseline p-Syk, p-Erk, and p-Akt in all three in CH12-IgM and CH12-IgE cells, with higher levels of each in CH12-IgG1 cells (*SI Appendix*, Fig. S4*E*). These results suggest that intrinsic differences in isotype-specific BCR signaling likely contribute to B cell behaviors.

Weaker Developmental Ig Repertoire Selection in IgG and IgE B Cells. To explore the degree to which IgG1 and IgE may influence selection of preimmune Ig repertoires, we sorted pro-B and follicular B cells from *IghWTVJκ5*, *Ighγ1/γ1VJκ5*, and *Ighε/εVJκ5* mice for Ig repertoire sequencing (*SI Appendix*, Fig. S5 *A* and *B*). Analysis showed grossly similar V_H segment use patterns in pro-B cells from each of the genotypes (Fig. 2*K* and *SI Appendix*, Fig. S5*C*). However, the selection patterns between pro-B and follicular B cells varied. In this regard, the V_H segment V_H5–*2* (also known as *81x*), is known to be highly used in pro–B cell VDJ_H assemblies, but is strongly selected against during B cell development (30). This results in more rare V_H5–*2* use in mature B cells, presumably due to its autoreactivity (31, 32). We see V_H5–*2* highly represented in pro-B cells from all genotypes (Fig. 2*K* and *SI Appendix*, Figs. S5*C* and S6 *A*–*C*, brown box in *Upper Left* corner of the treemap plots), and it is selected against in follicular B cells from *IghWTVJκ5* and *Ighγ1/γ1VJκ5* mice, indicating that this aspect of selection is grossly intact in *Ighγ1/γ1VJκ5* mice. However, the V_H5–*2* gene segment is still the highest used in *Ighε/εVJκ5* follicular B cells (Fig. 2*K* and *SI Appendix*, S5*C* and S6 *A*–*C*). This may indicate selection of autoreactive cells capable of overcoming developmental blockade due to otherwise weak signaling. An alternative possibility is that BCR expression may be insufficient to arbitrate BCR-mediated and/or ligand-mediated developmental selection. The fact that overall V_H use patterns between pro-B and follicular B cells in *Ighε/εVJκ5* is significantly more highly correlated than what is seen in the others suggests the latter is more likely (*SI Appendix*, Fig. S6 *D* and *E*). Analysis of BM pro-B and splenic follicular B cell V_H gene segment use in *Ighγ1/γ1VJκ5* mice also showed a nonsignificant trend toward preservation of the pro–B cell repertoire profile compared to *IghWTVJκ5* mice. Postsort cell analysis indicates the preservation of pro–B cell repertoires is not due to early B-lineage cell contamination (*SI Appendix*, Fig. S5*A*).

IgG1 and IgE B Cells Are Moderately and Severely Biased, Respectively, Against the mIg Alternatively Spliced mRNA Variant. We asked whether differences in alternatively spliced mRNA might contribute to the different BCR density rankings observed in IgG1, IgE, and IgM B cells. Because alternative promoter use can influence alternative splicing (33), as well as mRNA stability (34), we developed an absolute qPCR assay to measure absolute amounts of productive sIg and mIg mRNA splice variants by comparing to a known amount of a standard. Productive mRNA transcripts encoding the VDJ_H exon together with the C_H exons are generated from V_H promoters 5′ to the VDJ_H exon. Germline (GL) C_H transcripts are initiated downstream of the VDJ_H exon from a noncoding exon 5′ to each C_H region (called the I_H exon) present at each *Igh* isotype. B cells constitutively produce transcripts from both V_H and Iμ promoters, while the other I_H region promoters (e.g., *Iγ1*, Iε) are induced upon activation. GL transcripts from I_H promoters are capped, polyadenylated, and spliced. Previous measurements of sIg and mIg splice variants using relative qPCR assessments of 3′ ends of sIg and mIg mRNA have not accounted for possible differences of these different promoters on splicing bias (8, 27).

We amplified either V_H or I_H promoter-driven transcripts from wild-type B cells activated for IgG1 and IgE CSR in vitro before using absolute qPCR to measure sIg and mIg variants from each pool against their respective standards (*SI Appendix*, Fig. S7). RNA transcripts produced from *Iμ* and *Iγ1* promoters were relatively more biased toward mIg compared with their V_H promoter counterparts (*SI Appendix*, Fig. S8 *B*–*D*). In contrast, the sIg/mIg ratio was similar between *Iε* and its V_H promoter counterpart (*SI Appendix*, Fig. S8*C*). CSR to IgE and IgG1 results in the juxtaposition of *Iμ* to *Cε* or *Cγ1*, respectively. In addition, downstream CSR can juxtapose *Iγ1* to *Cε* (35). We found that *Iμ*-driven transcripts were also relatively biased toward mIg for Iμ-Cγ1 and Iμ-Cε transcripts compared with corresponding V_H transcripts, and that mIg was also relatively favored in the context of Iγ1-Cε transcripts (*SI Appendix*, Fig. S8 *B*–*D*). These results suggest that promoter use influences alternative splicing biases in the *Igh* locus, thus supporting a need to isolate and assess transcripts from V_H promoters to quantify mRNA variants relevant for protein production.

We used V_H promoter-driven transcript amplification and absolute qPCR assay to assess sIg/mIg mRNA ratios in B cell subsets from *Ighε/εVJκ5* and *Ighγ1/γ1VJκ5* mice. We found that pro-B cells from *Ighε/ε* mice make several hundred-fold higher sIgε than mIgε (Fig. 3*A* and *SI Appendix*, Fig. S9*A*). Pro-B cells from *Ighγ1/γ1VJκ5* mice are also biased to the sIgγ1 mRNA variant at a level of ∼40-fold over mIgγ1 mRNA (Fig. 3*A* and *SI Appendix*, Fig. S9*A*). The sIg/mIg ratios from *Ighγ1/γ1VJκ5* and *Ighε/εVJκ5* splenic follicular IgG1 and IgE B cells, respectively, showed similar levels to those found in pro-B cells from the respective mice (Fig. 3*A*). Igμ mRNA in wild-type pro-B cells is biased toward the mIgμ splice variant, with an sIgμ/mIgμ of ∼0.4, while the sIgμ/mIgμ increased to an ∼1:1 ratio at the mature naïve B cell stage (Fig. 3*B*).

To evaluate IgH isotype mRNA splicing bias in wild-type cells, we stimulated wild-type B cells to undergo CSR to IgE and IgG1 in vitro (*SI Appendix*, Fig. S9*B*). We found that activated, switched B cells are heavily biased toward the sIgε and sIgγ1 splice variants, with Igε mRNA being the most biased toward sIg and Igμ being the least (Fig. 3*B*). To determine if similar splicing bias can be detected in memory B cells, we immunized the AID-cre-ERT2 Rosa26-loxP-EYFP memory cell reporter mice (6) with sheep red blood cells and sorted IgM$^+$ and IgG1$^+$ memory (EYFP$^+$ CD38$^+$GL7$^-$) B cells to measure splice bias (Fig. 3*C*) (no IgE$^+$ B cells detected). We found an ∼100-fold higher sIg/mIg ratio in IgG1$^+$ B cells compared with IgM$^+$ memory B cells (Fig. 3*D*), which remains at an approximate 1:1 ratio (Fig. 3*D*). Together, these data indicate that the general splicing bias hierarchy found in *Ighγ1/γ1VJκ5* and *Ighε/εVJκ5* mice is also found in IgE and IgG1 cells from wild-type B cells.

Ectopic mIgγ1 or mIgε Rescues B Cell Development in *Ighε/ε*, *Ighγ1/γ1*, and μMT Pro-B Cells. To determine the degree to which developmental blockage at pro–B cell stage is a result of low density of mIgε and mIγ1 in *Ighε/ε* and *Ighγ1/γ1* mice, we retrovirally transduced the membrane form of IgE and IgG1, or empty vector, in developing B-lineage cells ex vivo from *Ighε/ε* and *Ighγ1/γ1* mice, and measured *Igκ* rearrangement. We included developing B-lineage cells from μMT mice, which have a similar B cell developmental blockade due to inability to produce mIgμ (22). Pro-B cells were transduced with vectors expressing GFP alone, or with mIgM, mIgG1, or mIgE followed by measurement of *Igκ* assembly and Igκ protein expression. *Ighε/ε*, *Ighγ1/γ1*, and μMT pro-B cells transduced with GFP alone had minimal *Igκ* assembly and protein expression; however, enforced expression of mIgE and mIgG1 was able to induce *Igκ* gene assembly (Fig. 4 *A*–*C*). This resulted in surface Igκ expression in pro-B cells from all three genotypes,

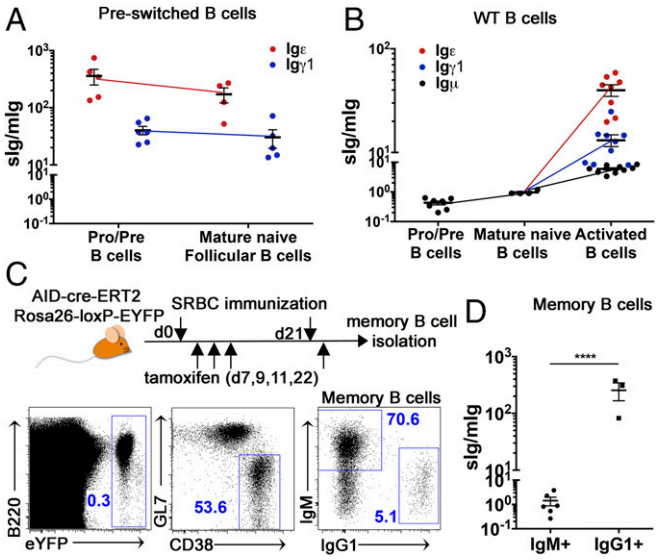

Fig. 3. Moderate and severe bias to sIg in IgG1 and IgE cells, respectively. (*A*) Dot graph showing the ratio of sIg/mIg mRNA expression for Igε (red) and Igγ1 (blue) from B220$^+$ BCR$^-$ bone marrow (pro/pre) and mature follicular (B220$^+$ CD93$^-$ BCR$^+$ CD21^{int} CD23^{hi}) B cells from *Igh*ε/ε (red) and *Igh*γ1/γ1 (blue) mouse spleens (n = 4–5). The sIg and mIg levels, as well as total Ig mRNA levels were determined by absolute qPCR using known levels of standards. (*B*) Dot graph showing the ratio of sIg/mIg for Igμ (black), Igε (red), and Igγ1 (blue) from the indicated B cells isolated from wild-type (WT) mice. Pro/pre B cells are from B220$^+$ BCR$^-$ bone marrow. Mature B cells are from magnetically purified B220$^+$ splenic cells. Activated B cells were derived by stimulation of magnetically purified B220$^+$ splenic cells with anti-CD40 antibody plus IL-4 for 4 d (n = 4–9). (*C*) Schematic outline (above) of AID-cre-ERT2 Rosa26-loxP-EYFP mice immunized with sheep red blood cells (SRBCs) and induced with tamoxifen as outlined. FACS plots (*Below*) show gating strategy for flow cytometric sorting of IgM$^+$ and IgG1$^+$ memory (EYFP$^+$ CD38$^+$ GF7$^-$) B cells (n = 6). (*D*) Graph showing sIg/mIg mRNA ratios of IgG1$^+$ and IgM$^+$ of memory B cells shown in *C* by the absolute qPCR method described in *A*. Dots represent individual mice (n = 6). The mIgG1 mRNA level was below detection in three IgG1$^+$ memory cell samples. ****P < 0.000, two-tailed t test. Summary data are means ± SEM. See also *SI Appendix*, Figs. S7–S9.

reaching significance in *Igh*ε/ε, and μMT pro-B cells, but not in *Igh*γ1/γ1 pro-B cells, likely due to the higher background from natural assembly and expression of Igκ in these mice (*SI Appendix*, Fig. S10*A*).

As the mIgH constructs contained a GFP reporter controlled by an internal ribosomal entry site (IRES), GFP expression can provide an indicator of amount of mIgH RNA. Cells gated based on low to high expression of GFP showed an expression-dependent increase of the percentage of cells expressing Igκ. (Fig. 4 *D* and *E*). These results indicate that both IgE and IgG1 can compensate for IgM in delivering a BCR signal sufficient to induce B-lineage maturation in a density-dependent fashion. Because SLC interaction with IgH is known to be functionally required for *Ig*κ assembly (36), these results also suggest that IgG1 and IgE can functionally interact with SLC. These findings suggest that insufficient BCR density is likely a contributing factor in the BM blockade seen in *Igh*ε/ε and *Igh*γ1/γ1 mice.

While mIgE and mIgG1 could both rescue Igκ production, mIgM appeared to have an advantage in producing a higher percentage of Igκ$^+$ cells, which was more apparent when tested in the context of *Igh*γ1/γ1 and μMT pro-B cells (Fig. 4*E*). We found that this mIgM advantage may be related to the ability of mIgM to induce proliferation to a greater extent than mIgG1 or mIgE in the context of pro-B cells from *Igh*γ1/γ1 or *Igh*ε/ε mice retrovirally transduced with mIgH (*SI Appendix*, Fig. S10 *B* and *C*). The advantage seen by mIgM in inducing more proliferation suggests that isotype-intrinsic BCR signaling may contribute as well to the BM blockade seen in *Igh*ε/ε and *Igh*γ1/γ1 mice.

Strengthened PI3K Signaling Can Generate a Memory Response Mediated by IgE$^+$ B Cells. Immunologic IgE memory responses are unlikely to be housed in IgE B cells themselves, whereas IgG1 B cells can function in both IgG1 and IgE memory (8, 12). To determine the degree to which IgG1 and IgE B cells in *Igh*γ1/γ1 and *Igh*ε/*εVJ*κ5 mice can participate in a conventional immune response to produce antigen-specific antibodies to immunization, we immunized them with ovalbumin (OVA) and assessed IgH isotype-specific serum anti-OVA antibodies. We rechallenged the mice as well to test whether a functional memory response could be detected. For *Igh*γ1/γ1 mice, we detected IgG1 and IgE anti-OVA responses similar to *Igh*γ1/*WT* heterozygotes with immunization, with levels increasing in magnitude after rechallenge for IgE responses (Fig. 4 *F* and *G*), indicating that the IgG1 cells are competent for germinal center entry and selection as well as CSR to IgE upon activation as expected. In contrast, immunization of *Igh*ε/*εVJ*κ5 mice did not induce any detectable anti-OVA IgE response (Fig. 4*H*), consistent with previous reports of rapid death of IgE$^+$ cells upon activation (8, 9).

We crossed *Igh*ε/*εVJ*κ5 mice to *Cd19*cre *Pten*$^{c/c}$ mice for conditional PTEN deletion in B cells with the goal to examine the degree to which strengthened BCR signaling could rescue a functional memory response for IgE$^+$ B cells. PTEN is a negative regulator of PI3K signaling, which is downstream of BCR. When *Pten* is conditionally deleted in B cells, BCR signaling is bypassed and B cells act as though they are receiving stronger BCR signals (37). CD19 has also been shown to interact with IgE and negatively regulate IgE responses (16). *Igh*ε/*εVJ*κ5 *Cd19*cre$^+$ *Pten*$^{c/c}$ mice have over fivefold more splenic B cells compared with controls at baseline (Fig. 4 *I*–*K*), consistent with previous reports of a role of B cell *Pten* deletion rescuing B cell numbers in the setting of insufficient BCR expression (37). After immunization, clear anti-OVA IgE responses were observed in several Igh ε/*εVJ*κ5 mice with B cell *Pten* deletion that increases in magnitude upon rechallenge, while five out of six Igh ε/*εVJ*κ5 cre-negative control mice showed no sustained response (Fig. 4*L*). IgE responses have recently been shown to be increased in the setting of CD19 haploinsufficiency via an unclear mechanism (16). Since *Cd19*cre mice are also haploinsufficient for CD19, this may also contribute to the increased IgE responses in *Igh*ε/*εVJ*κ5 *Cd19*cre$^+$ *Pten*$^{c/c}$ mice. Because the magnitude of the *Cd19* haploinsufficiency is mild (16), lower CD19 expression alone in *Cd*19cre mice is unlikely to explain the large effects observed (Fig. 4*L*). These results suggest that the lack of functional memory cell capabilities within IgE$^+$ cells may be restored by B cell *Pten* deletion, implying that weak BCR signaling by IgE, potentially provided by minimal BCR density, plays a key role in limiting IgE$^+$ activation and memory cell functional capacity.

Discussion

IgH isotype plays a major role in defining function of secreted antibodies and can influence BCR function to regulate B cell fate when expressed as mIg. Our data are consistent with a concept that individual IgH isotypes are linked to C_H-specific control elements that contribute to isotype-specific BCR dosage regulation.

Alternative RNA splicing was first identified in Igμ transcripts (38–40) and was later shown to be a widespread mechanism of gene regulation (41). Alternative splicing for *Ig*μ favors mIg during early B cell development and in naïve B cells, whereas sIg is favored upon activation (2, 42). The sIg/mIg mRNA ratios of *C*ε and *Cγ1* do not appear to be susceptible to this regulation as they favor the sIg splice variant at the expense of mIg, regardless of cell stage. For *C*ε, nonconsensus polyadenylation sequences downstream of membrane exons have been shown to underlie

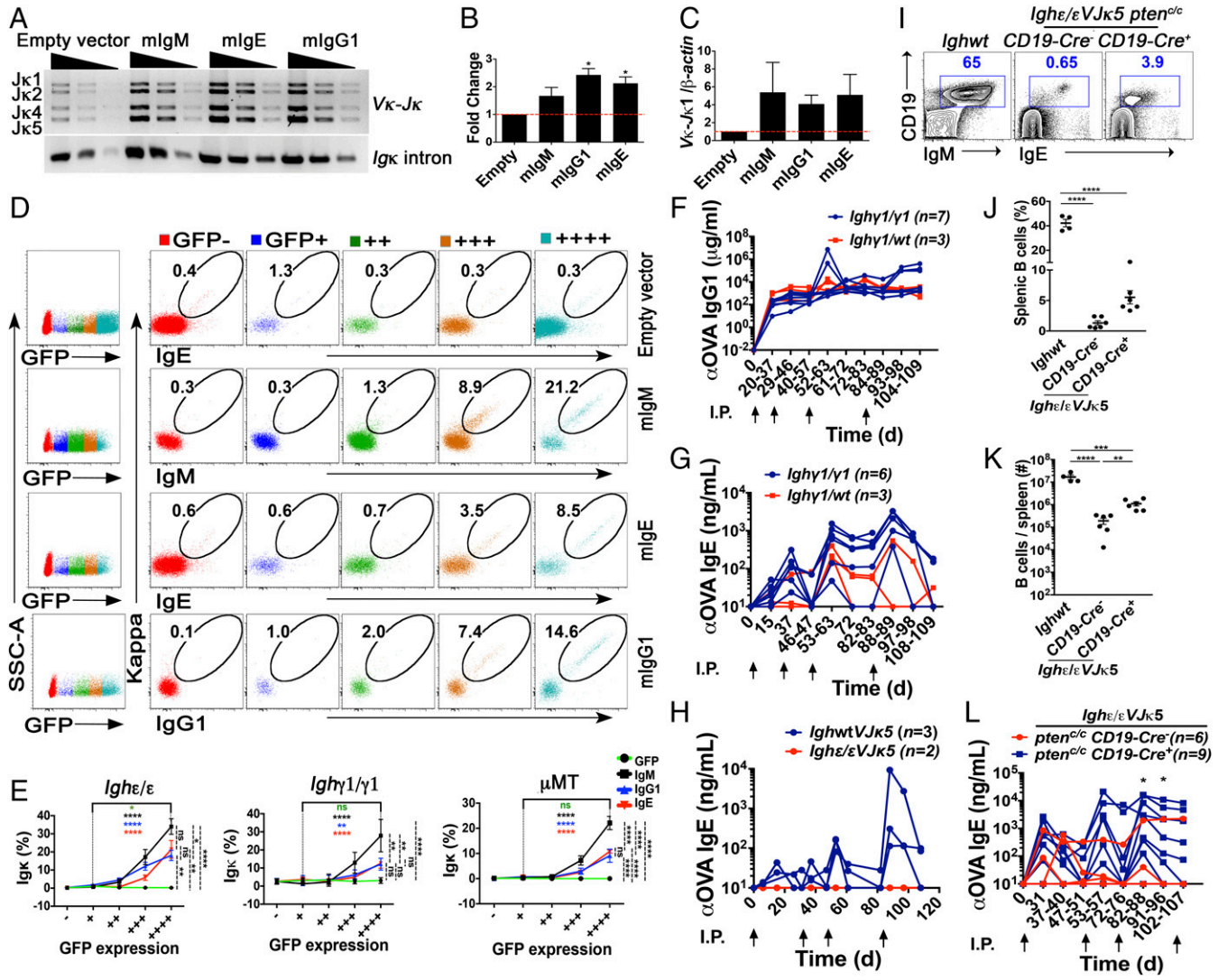

Fig. 4. Overexpression of mIgH rescues B cell development in *Igh*ε/ε, *Igh*γ1/γ1, and μMT pro-B cells, and *Pten* deletion can generate a memory response mediated by IgE$^+$ B cells. (*A*) Image of semiquantitative PCR results to detect *V*κ to *J*κ1 assemblages in *Igh*ε/ε pro/pre-B cells transduced with the indicated retroviral vectors. Threefold dilutions are shown. Amplification of an intronic *Ig*κ sequence was used as a loading control. Result is representative of three experiments. Bands corresponding to rearrangements to various *J*κ segments are indicated on the *Left*. (*B*) Densitometry analysis of the semiquantitative PCR data in *A* with ImageJ for three repeated experiments. Shown are fold changes relative to the empty vector control ($n = 3$), $^*P < 0.05$, one sample *t* test. Summary data are means ± SEM. (*C*) Quantitative PCR analyses of *V*κ to *J*κ1 rearrangement relative to intronic β-*actin* DNA in *Igh*ε/ε pro/pre-B cells transduced with the indicated retroviral vectors. Shown are fold changes relative to the empty vector control. Summary data are means ± SEM. While each mIgH expression vector was at least twofold higher than the empty vector control, one-sample *t* tests showed no significant differences. (*D*) Representative FACS analysis of Igκ and IgE, IgM, or IgG1 surface expression in *Igh*ε/ε pro/pre-B cells transduced with the indicated retroviral vectors. Numbers indicate percentage of surface Igκ$^+$ IgH$^+$ on live CD19$^+$ B cells, which express from no GFP to highest GFP, indicated by increasing number of "+" signs ($n = 6$). (*E*) Quantification of surface Igκ$^+$ on live CD19$^+$ B cells which express from no GFP to highest GFP after retroviral transduction in *Igh*ε/ε, *Igh*γ*1*/γ*1*, and μMT pro/pre-B cells ($n = 4$–6). $^*P < 0.05$, $^{**}P < 0.01$, $^{****}P < 0.0001$; one-way ANOVA followed by Tukey's post hoc test. Data are mean values ± SEM. (*F* and *G*) Graph of ELISA data showing ovalbumin (OVA)-reactive IgG1 (*F*) and IgE (*G*) in sera from *Igh*γ1/γ1 (blue) and heterozygous *Igh*γ*1/WT* (red) mice immunized and boosted intraperitoneally with OVA at the time intervals shown by the upward arrows. Fisher's exact test showed no significant differences. (*H*) Graph of ELISA data showing OVA-reactive IgE in sera from WT (blue) and *Igh*ε/ε*VJκ5* (red) mice immunized and boosted intraperitoneally with OVA at the times shown by the upward arrows. No response was observed in two *Igh*ε/ε*VJκ5* mice, whereas all three WT mice responded. (*I*) FACS plots showing splenic lymphocytes analyzed for CD19 and IgE expression from the indicated mice ($n = 4$–6). (*J* and *K*) Summary dot graphs showing percentages (*J*) and total number (*K*) of splenic B cells from the indicated mice. Dots represent individual mice ($n = 4$–6). $^{**}P < 0.01$, $^{***}P < 0.001$, $^{****}P < 0.0001$; one-way ANOVA followed by Tukey's post hoc test. Data are mean values ± SEM. (*L*) Graph of ELISA data showing OVA-reactive IgE in sera from *Igh*ε/ε*VJκ5 Pten*$^{c/c}$*Cd19*cre$^-$ (blue) and *Igh*ε/ε*VJκ5 Pten*$^{c/c}$*Cd19*cre$^+$ (red) mice immunized and boosted intraperitoneally with OVA at the time intervals shown by the upward arrows. The *y* axis shows apparent binding in milligrams/milliliters or nanograms/milliliters as indicated based on comparisons to a standard anti-ovalbumin IgG1 or anti-ovalbumin IgE antibody. Number of mice used in each immunization is shown. $^*P < 0.05$, Fisher's exact test. See also *SI Appendix*, Fig. S10.

bias against mIg splice forms due to higher efficiency polyadenylation at a consensus site upstream of the membrane exons (27). The *Cγ1* locus has consensus polyadenylation signals both upstream and downstream of its membrane exons, implicating other regulatory mechanisms involved in producing sIg bias observed in IgG1 B cells. While splicing plays a role in *Igh* gene expression, other features may contribute to IgH isotype-specific BCR density regulation, such as mRNA turn over, translation, surface protein stability, intrinsic signaling differences, as well as endocytosis and BCR recycling. In addition, while IgM appears to be produced

with relatively higher mIg/sIg compared with other IgH isotypes, BCR density has the potential to be even greater when IgD is expressed in addition to IgM, as occurs in mature naïve B cells and in some IgM$^+$ memory B cells.

Our finding that retrovirally transduced mIgE and mIgG1 can rescue B cell developmental progression in *Igh*ε/ε, *Igh*γ1/γ1, as well as μMT mice in an expression density-dependent fashion suggests that there may be more functional overlap of autonomous signaling between IgH isotypes than previously anticipated. However, our data are not inconsistent with the concept that differences in autonomous signaling between IgH isotypes contribute to isotype-specific differences in BCR function. BCR dosage levels and autonomous signaling differences likely act together to influence BCR function. Isotype-specific BCR dosage can impact B cell fate by defining signaling needs required to reach functional thresholds through ligand engagement (43). For example, B cells with more dilute BCR isotypes may require higher affinity and/or more cognate antigen availability to reach an integrated BCR signal strength that is similar to cells endowed with higher BCR density (24). The observation that autoreactive V_H*5–2* was found to be dominant in *Igh*ε/ε*VJ*κ5 follicular B cells is consistent with this concept, in that rare IgE cells may have been allowed to develop due to continuous recognition of a putative self-antigen. However, because V_H use frequencies between *Igh*ε/ε*VJ*κ5 pro-B cells and follicular IgE B cells are so highly correlated (*SI Appendix*, Fig. S6*E*), with V_H*5–2* favored in both, an alternative explanation is that dilute IgE (and perhaps to a lesser extent, IgG1) BCR may render cells relatively deaf to the normal ligand-mediated signals that usually accompany early B cell maturation, resulting in preservation of the pro–B cell V_H use pattern (*SI Appendix*, Fig. S6).

While we know of no other reports of IgE preswitched models, other work has generated preswitched models for IgG (44–47), most with monoclonal Ig specificities. Since Ig specificity alone can substantially impact B cell development (48, 49), it is not clear what aspects of development are due to IgH isotype versus Ig specificity in monoclonal models (44–46, 50). A polyclonal IgG1 preswitched model, called IgHγ1μ mice, was produced wherein the intronic polyA site (that regulates splicing to the secreted IgG variant) was deleted to enhance mIgG1 over sIgG1 production (47). In this setting, the IgHγ1μ mice have normal peripheral B cell numbers compared with wild-type controls (47), whereas our *Igh*γ1/γ1 mice are B cell lymphopenic, harboring over 10-fold less peripheral B cells than wild-type controls (Fig. 1*E*). This comparison is consistent with the concept that BCR expression, at least at the mRNA level, plays a role in influencing B cell numbers. The observation of an early BM developing B-lineage cell blockade in IgHγ1μ mice suggests that aspects of IgG1 intrinsic signaling contribute to similar blockage in *Igh*γ1/γ1 mice, consistent with our finding that mIgM provides a pre–B cell proliferative advantage (*SI Appendix*, Fig. S10 *B* and *C*). The fact that the blockade in IgHγ1μ mice is much less severe (47) suggests that BCR expression plays a role as well at this stage of development.

Isotype-specific BCR density limits may contribute to functional differences observed in IgG1 and IgE B cells under normal settings, such as limited entry into the memory B cell compartments. The moderate and severe limitations of mIg production for IgG1 and IgE, respectively, are in line with findings showing that IgM-expressing B cells appear to enter the memory compartment at a higher level compared with IgG1-expressing B cells (6, 7, 10), and that IgE-expressing memory B cells are essentially nonexistent (8, 9, 12). In addition, our finding that functional antigen-specific IgE memory carried out by IgE-expressing B cells in the setting of *Cd19* hemizygosity and *Pten* deficiency, is consistent with the concept that weak signaling from IgE BCRs limits IgE memory B cell formation. We conclude that IgH isotype-specific BCR dosage control is a regulatory mechanism in the B cell system.

Materials and Methods

Mice. The Children's Hospital Boston Animal Care and Use Committee (IACUC) and the Warren Alpert Building, Boston, IACUC approved all experiments. Doxycycline-inducible reprogrammable mice used in these experiments have been described previously (46, 51). Splenic B cells from reprogrammable mice were isolated and CSR to IgG1 and IgE was induced as described previously (46). Details can be found in *SI Appendix*. The *Igh*γ/γ*1*, *IghWT*, *Igh*ε/ε, and *VJ*κ5 variants were all maintained on a mixed 129.B6 background. The μMT mice (*B6.129S2-Ighm^{tm1Cgn}/J*), *Pten$^{c/c}$* (*B6.129S4-Pten^{tm1Hwu}/J*) mice and *Cd19*cre (*B6.129P2(C)-Cd19tm1(cre)Cgn/J*) mice were purchased from The Jackson Laboratory. The *Rag2$^{-/-}$*, described previously (52), was provided by Frederick Alt, Boston Children's Hospital, Boston. *Aid$^{-/-}$* mice were provided by Honjo and colleagues (53). Unless otherwise noted, all mice were housed at the Boston Children's Hospital animal facility under specific pathogen-free (SPF) conditions. AID-cre-ERT2 Rosa26-loxp-EYFP mice were housed in the Warren Alpert Building under SPF conditions. See *SI Appendix* for further details.

Cell Isolation and Flow Cytometry. BM cells were flushed from femurs and tibias with ice-cooled staining buffer (PBS supplemented with 2% FBS). Spleen cell suspensions were obtained by gently teasing spleens onto a 70-μm cell strainer. Erythrocytes were depleted using red blood cell lysis buffer (Sigma). Cells were counted using a hemocytometer with exclusion of dead cells with Trypan blue dye. Cells were stained with fluorophore or biotin-conjugated antibodies as described (54, 55) where indicated. The cell sorting was performed on a FACSAria II flow cytometer (BD Biosciences). For the in vitro CSR experiments and the allelic exclusion experiments, staining for IgM, IgG1, and IgE for intracytoplasmic IgH expression was done by using trypsinization followed by fixation/permeabilization as described (54, 55). Data analysis was performed with FlowJo software (v9.9.4). See *SI Appendix* for further details.

Cell Culture and CSR Assay. Splenic and BM cells were isolated by B220 positive selection via magnetic columns (Miltenyi Biotech) according to manufacture instructions. The CH12 B cell line was previously described (56) and provided by Frederick Alt. Cells were cultured in RPMI (Corning/Cellgro) supplemented with 2 mM L-glutamine (Gibco), 100 units/mL penicillin and 100 μg/mL streptomycin (Gibco), 0.1 mM nonessential amino acids (Gibco), 20 mM Hepes (Gibco), 0.1 mM β-mercaptoethanol (Sigma-Aldrich) and 15% FBS (HyClone). CSR to IgG1 and IgE was performed as described (46). For pro/pre–B cell enrichment, B220$^+$ BM cell cultures were stimulated with 20 ng/mL IL-7 (R&D Systems) for 3–4 d. Immature B cells were excluded via BCR negative selection using biotinylated anti-mouse IgM, IgG1, or IgE followed by anti-biotin magnetic columns (Miltenyi Biotech) according manufacture instructions. Pro/pre–B cell populations showed purity >95%.

Immunization. Male and female *Igh*γ*1/*γ*1*, *Igh*γ*1/WT*, *Igh*ε/ε*VJ*κ5, *Igh*ε/ε*VJ*κ5 *Pten$^{c/c}$Cd19*cre$^-$, and *Igh*ε/ε*VJ*κ5 *Pten$^{c/c}$Cd19*cre$^+$ mice at 6–8 wk were immunized with 50 μg per mouse chicken OVA (Sigma-Aldrich) at days 0, 21, 47, and 73. *AID-cre-ERT2 Rosa26-loxp-EYFP* mice were immunized with 2 × 10^8 sheep red blood cells (Colorado Serum Company) at days 0 and 21. AID expression is induced by oral administration with 15 mg tamoxifen per mouse per time point at days 7, 9, 11, and 22.

ELISA. Total serum IgE and IgG1 were quantified by sandwich ELISA with the following antibodies: purified anti-mouse IgE (R35-72, BD Biosciences) and alkaline phosphatase conjugated anti-mouse IgE (23G3, Southern Biotech); purified anti-mouse IgG1 (SB77e, Southern Biotech), and alkaline phosphatase conjugated anti-mouse IgG1 (X56, BD Biosciences). To measure serum OVA-specific IgE and IgG1 by ELISA, plates were coated with 20 μg/mL of chicken OVA (Sigma-Aldrich), followed by blocking and incubation with mouse serum dilutions. The same detection antibodies described earlier were used. In both assays, standard curves were generated with serial two- or fourfold dilutions of OVA-specific mouse IgE (Cayman Chemical) or OVA-specific mouse IgG1 (TOSG1C6, Biolegend). Phosphatase substrate tablets (Sigma-Aldrich) were used according to manufacture instructions.

Overexpression of mIgH in Pro-B Cells. The cDNAs for mIgM, mIgG1, and mIgE were prepared from the CH12 B cell line (mIgM) or CH12-derived B cell lines induced to undergo IgH CSR to IgG1 and IgE and cloned into the pMIG vector (Addgene). BM cells from *Igh*ε/ε, *Igh*γ1/γ1, and μMT mice were cultured in the presence of IL-7 (20 ng/mL). After 2–3 d, cultured BM cells were infected with GFP or mIgH-encoding retroviruses. After two additional days, culture medium was removed and cells were cultured in the presence of BAFF and

IL-4 for 3 d. Kappa chain rearrangement was analyzed by flow cytometry. See *SI Appendix* for further details.

Ig V_H Assembly Analysis. Threefold serial dilutions of genomic DNA (≈100 ng, 30 ng, and 10 ng) were used to perform PCR to analyze Ig heavy chain VDJ_H and Ig light chain Vκ-Jκ rearrangements. Two main V_H families were analyzed (7183 and J558) using primers described previously (57). Primers flanking exon 6 of the *Dlg5* gene were used as a loading control (*SI Appendix*, Table S1). Vκ-Jκ rearrangement products were PCR amplified using a degenerate Vκ and the Mar35 primers described previously (58). Primers in the Igκ intron were used as a loading control (*SI Appendix*, Table S1). *Vκ-Jκ1* rearrangement was also determined by quantitative PCR assay using the degenerate Vκ forward primer and a reverse primer complementary to sequences downstream of *Jκ1* (Jκ1–2R) as described previously (59, 60). Rearrangement levels measured by qPCR were normalized to the levels of β-*actin* DNA.

Total RNA Isolation and Gene Expression Analysis. Total RNA was extracted using the TRIzol method (Invitrogen), followed by treatment with RNase-free DNase (Qiagen) and RNeasy columns cleanup (Qiagen). Affymetrix Mouse 2.0 ST GeneChips microarray gene expression data were done with the Bioconductor package (R version 3.3.1, Bioconductor version 3.4). The raw data from the .CEL files were normalized and expression matrix was log transformed. Pearson's correlation coefficient (*r*) and fold change in expression level of various genes under different conditions were calculated based on the biweight average of three biological replicates.

Isolation and Measurement of Membrane Secretory IgH mRNA. Cell mRNA was isolated using Dynabeads mRNA DIRECT Micro Purification Kit (ambion/Life technologies), followed by DNA elimination with gDNA wipeout (Qiagen). cDNA was obtained using SuperScript III reverse transcription system (Invitrogen) using anchored Oligo$(dT)_{20}$ primers (Invitrogen). When V_H and I_H promoter-driven transcripts were analyzed, the RT step was performed with anchored oligo dT coupled to an universal sequence (*SI Appendix*, Table S1), followed by a PCR step to amplify either V_H or I_H promoter-driven transcripts. For V_H promoter transcripts, the V_H segment leader sequence (V_H leader Fw) was used as a forward primer. A mixture of forward primers against all four J_H regions (J_H1–4 Fw) were also used (*SI Appendix*, Table S1). For I_H promoter transcript amplification, Primers complementary to Iμ, Iε, or Iγ1 (Iμ2 Fw, Iε Fw or Iγ1 Fw) were used as forward primers; the reverse primer (UNV Rv) was the universal sequence that was appended to the poly T primer on the RT step. Levels were normalized by total μ, ε or γ1 transcripts using primers located in the shared constant exon. The following primers set were used: mμ, sμ and tμ; mε, sε and tε; mγ1, sγ1 and tγ1 (*SI Appendix*, Table S1). Absolute quantification was determined by standard curves with linearized pGEM plasmids expressing mIgM, sIgM, mIgE, sIgE, mIgG1 or sIgG1 genes cloned from CH12 cells (for IgM), as well as CH12s isolated after in vitro CSR to IgE (CH12-IgE) and IgG1 (CH12-IgG1). See *SI Appendix* information for further details.

Deep Sequencing. Pro-B and follicular B cell RNA was reverse-transcribed before heat inactivation of reverse transcriptase and primer removal using Uracyl DNA glycosylase. The glycosylase was then heat inactivated and the first cDNA strand was tagged with a unique molecular identifier (UMI) with one cycle of second strand DNA synthesis before removing residual primers with RNAClean XP beads. Nine cycles of preamplification were used to enrich the samples from *Ighγ1/γ1VJκ5* and *Ighε/εVJκ5* mice (due to low cell count) before first round PCR. Qiaquick PCR purification kit was used to purify the preamplification products. Subsequently, first round PCR added 5′ and 3′ adaptors to both ends of the amplicon and resulted in amplification of heavy chains using 25 cycles. For samples from *IghWTVJκ5* mice, purified barcoding products go directly to first round PCR without preamplification step. Second round PCR added Illumina linkers (P5 and P7) and sample barcodes in separate reactions using 17 cycles. All of the primers used for the deep sequencing are listed in *SI Appendix*, Table S1. Products were quantified on a Qubit fluorimeter, run on a fragment analyzer with amplicon regions and expected sizes confirmed. Samples were then pooled in equal amounts according to product concentration. The pooled products were then size selected on an agarose gel and purified by gel extraction. Purified, size-selected products were run on an Agilent Bioanalyzer to confirm appropriate profile and determination of average size. The final pools were quantitated using Qubit and diluted to 5 nM before further quantification by qPCR on a BioRad CFX Connect Real-Time System and pooled evenly. The pool was denatured and spiked with 15% nonindexed PhiX control library provided by Illumina and loaded onto the MiSeq V2 Nano flowcell at a concentration of 7 pM for cluster formation and sequencing. The PhiX control library provides a balanced genome for calculation of matrix, phasing and prephasing, which are essential for accurate basecalling. The libraries were sequenced from both ends of the molecules to a total read length of 250 nt from each end.

Sequencing Data Analysis. The sequences obtained from Illumina MiSeq deep sequencing (nano-run) were run through the standalone IgBlast software (version 1.4.0) to identify the V_H segment using reference sequences from IMGT. PCR repeats were filtered using unique molecular identifies (UMIs) applied during cDNA synthesis. Sequences with the same V_H and the same UMI were considered PCR repeats of the same mRNA. Only forward reads (R1) are used as the quality of R2 sequences was poor leading to low merge efficiency. Also, the CDR3 regions predicted were not reliable due to low quality intermittent nucleotides, which in-turn was required to rule out PCR repeats using the UMIs. By using only the UMIs and the V_H, we risk loosing some unique sequences attached to the same UMI at the cost of excluding all PCR repeats. The frequency of use of each V_H was calculated and compared for *IghWTVJκ5*, *Ighε/εVJκ5*, and *Ighγ1/γ1VJκ5* mice. All preprocessing and analysis was done using Bioconductor package v 3.4 (R version 3.3.1).

Data Availability. The raw sequence data for this study are accessible at the NCBI Sequence Read Archive (SRA) under BioProject accession number PRJNA394007 with BioSample accession numbers SAMN07347175–SAMN07347206.

Statistical Analysis. The *n* values in figures and figure legends indicate the number of individual mice, representing biologic replicates. Statistical analysis is described in the figure legends. Studies were not conducted blinded.

ACKNOWLEDGMENTS. We thank Christine Milcarek and Hans Oettgen for critical review of the manuscript and Soren Degn, Elisabeth Carroll, Rupa Kumari, Yuezhou Chen, Jiaxin Li, Colby Devereaux, John Manis, and Thomas Kepler for technical help and advice. This work is supported by the National Institutes of Health Grants AI121394 and AI1113217 (to D.R.W.), and National Council for Scientific and Technological Development (CNPq)/Science Without Borders Program, Brazil (to A.G.). D.R.W. holds a Career Award for Medical Scientists from the Burroughs Wellcome Fund and is supported by a New Investigator Award from Food Allergy Research & Education (FARE). This work was also supported by an anonymous gift.

1. Reth M (1992) Antigen receptors on B lymphocytes. *Annu Rev Immunol* 10:97–121.
2. Peterson ML (2011) Immunoglobulin heavy chain gene regulation through polyadenylation and splicing competition. *Wiley Interdiscip Rev RNA* 2:92–105.
3. Jung D, Giallourakis C, Mostoslavsky R, Alt FW (2006) Mechanism and control of V(D)J recombination at the immunoglobulin heavy chain locus. *Annu Rev Immunol* 24:541–570.
4. Tong P, Wesemann DR (2015) Molecular mechanisms of IgE class switch recombination. *Curr Top Microbiol Immunol* 388:21–37.
5. Nutt SL, Hodgkin PD, Tarlinton DM, Corcoran LM (2015) The generation of antibody-secreting plasma cells. *Nat Rev Immunol* 15:160–171.
6. Dogan I, et al. (2009) Multiple layers of B cell memory with different effector functions. *Nat Immunol* 10:1292–1299.
7. Pape KA, Taylor JJ, Maul RW, Gearhart PJ, Jenkins MK (2011) Different B cell populations mediate early and late memory during an endogenous immune response. *Science* 331:1203–1207.
8. He JS, et al. (2013) The distinctive germinal center phase of IgE+ B lymphocytes limits their contribution to the classical memory response. *J Exp Med* 210:2755–2771.
9. Yang Z, Sullivan BM, Allen CD (2012) Fluorescent in vivo detection reveals that IgE(+) B cells are restrained by an intrinsic cell fate predisposition. *Immunity* 36:857–872.
10. Gitlin AD, et al. (2016) Independent roles of switching and hypermutation in the development and persistence of B lymphocyte memory. *Immunity* 44:769–781.
11. Kometani K, et al. (2013) Repression of the transcription factor Bach2 contributes to predisposition of IgG1 memory B cells toward plasma cell differentiation. *Immunity* 39:136–147.
12. Erazo A, et al. (2007) Unique maturation program of the IgE response in vivo. *Immunity* 26:191–203.
13. Pogue SL, Goodnow CC (2000) Gene dose-dependent maturation and receptor editing of B cells expressing immunoglobulin (Ig)G1 or IgM/IgG1 tail antigen receptors. *J Exp Med* 191:1031–1044.
14. Roth PE, et al. (1993) Immunoglobulin gamma 2b transgenes inhibit heavy chain gene rearrangement, but cannot promote B cell development. *J Exp Med* 178:2007–2021.
15. Martin SW, Goodnow CC (2002) Burst-enhancing role of the IgG membrane tail as a molecular determinant of memory. *Nat Immunol* 3:182–188.
16. Haniuda K, Fukao S, Kodama T, Hasegawa H, Kitamura D (2016) Autonomous membrane IgE signaling prevents IgE-memory formation. *Nat Immunol* 17:1109–1117.
17. Laffleur B, et al. (2015) Self-restrained B cells arise following membrane IgE expression. *Cell Rep* S2211-1247(15)00048-0.

18. Poggianella M, Bestagno M, Burrone OR (2006) The extracellular membrane-proximal domain of human membrane IgE controls apoptotic signaling of the B cell receptor in the mature B cell line A20. *J Immunol* 177:3597–3605.
19. Dal Porto JM, et al. (2004) B cell antigen receptor signaling 101. *Mol Immunol* 41: 599–613.
20. Kitamura D, Rajewsky K (1992) Targeted disruption of mu chain membrane exon causes loss of heavy-chain allelic exclusion. *Nature* 356:154–156.
21. Lutz J, et al. (2011) Pro-B cells sense productive immunoglobulin heavy chain rearrangement irrespective of polypeptide production. *Proc Natl Acad Sci USA* 108: 10644–10649.
22. Kitamura D, Roes J, Kühn R, Rajewsky K (1991) A B cell-deficient mouse by targeted disruption of the membrane exon of the immunoglobulin mu chain gene. *Nature* 350: 423–426.
23. Tellier J, et al. (2016) Blimp-1 controls plasma cell function through the regulation of immunoglobulin secretion and the unfolded protein response. *Nat Immunol* 17:323–330.
24. Kouskoff V, Lacaud G, Pape K, Retter M, Nemazee D (2000) B cell receptor expression level determines the fate of developing B lymphocytes: Receptor editing versus selection. *Proc Natl Acad Sci USA* 97:7435–7439.
25. Wang LD, et al. (2004) Selection of B lymphocytes in the periphery is determined by the functional capacity of the B cell antigen receptor. *Proc Natl Acad Sci USA* 101:1027–1032.
26. Gaudin E, et al. (2004) Positive selection of B cells expressing low densities of self-reactive BCRs. *J Exp Med* 199:843–853.
27. Karnowski A, Achatz-Straussberger G, Klockenbusch C, Achatz G, Lamers MC (2006) Inefficient processing of mRNA for the membrane form of IgE is a genetic mechanism to limit recruitment of IgE-secreting cells. *Eur J Immunol* 36:1917–1925.
28. Venkitaraman AR, Williams GT, Dariavach P, Neuberger MS (1991) The B-cell antigen receptor of the five immunoglobulin classes. *Nature* 352:777–781.
29. Rickert RC (2013) New insights into pre-BCR and BCR signalling with relevance to B cell malignancies. *Nat Rev Immunol* 13:578–591.
30. Huetz F, Carlsson L, Tornberg UC, Holmberg D (1993) V-region directed selection in differentiating B lymphocytes. *EMBO J* 12:1819–1826.
31. Bellon B, et al. (1987) High frequency of autoantibodies bearing cross-reactive idiotopes among hybridomas using VH7183 genes prepared from normal and autoimmune murine strains. *J Clin Invest* 79:1044–1053.
32. Chen X, Kearney JF (1996) Generation and function of natural self-reactive B lymphocytes. *Semin Immunol* 8:19–27.
33. Xin D, Hu L, Kong X (2008) Alternative promoters influence alternative splicing at the genomic level. *PLoS One* 3:e2377.
34. Ayoubi TA, Van De Ven WJ (1996) Regulation of gene expression by alternative promoters. *FASEB J* 10:453–460.
35. Zhang T, et al. (2010) Downstream class switching leads to IgE antibody production by B lymphocytes lacking IgM switch regions. *Proc Natl Acad Sci USA* 107:3040–3045.
36. Miyazaki T, Kato I, Takeshita S, Karasuyama H, Kudo A (1999) Lambda5 is required for rearrangement of the Ig kappa light chain gene in pro-B cell lines. *Int Immunol* 11: 1195–1202.
37. Srinivasan L, et al. (2009) PI3 kinase signals BCR-dependent mature B cell survival. *Cell* 139:573–586.
38. Cushley W, Coupar BE, Mickelson CA, Williamson AR (1982) A common mechanism for the synthesis of membrane and secreted immunoglobulin alpha, gamma and mu chains. *Nature* 298:77–79.
39. Early P, et al. (1980) Two mRNAs can be produced from a single immunoglobulin mu gene by alternative RNA processing pathways. *Cell* 20:313–319.
40. Alt FW, et al. (1980) Synthesis of secreted and membrane-bound immunoglobulin mu heavy chains is directed by mRNAs that differ at their 3′ ends. *Cell* 20:293–301.
41. Smith CW, Patton JG, Nadal-Ginard B (1989) Alternative splicing in the control of gene expression. *Annu Rev Genet* 23:527–577.
42. Park KS, et al. (2014) Transcription elongation factor ELL2 drives Ig secretory-specific mRNA production and the unfolded protein response. *J Immunol* 193:4663–4674.
43. Geisberger R, Lamers M, Achatz G (2006) The riddle of the dual expression of IgM and IgD. *Immunology* 118:429–437.
44. Dougan SK, et al. (2012) IgG1+ ovalbumin-specific B-cell transnuclear mice show class switch recombination in rare allelically included B cells. *Proc Natl Acad Sci USA* 109: 13739–13744.
45. Dougan SK, et al. (2013) Antigen-specific B-cell receptor sensitizes B cells to infection by influenza virus. *Nature* 503:406–409.
46. Wesemann DR, et al. (2012) Reprogramming IgH isotype-switched B cells to functional-grade induced pluripotent stem cells. *Proc Natl Acad Sci USA* 109:13745–13750.
47. Waisman A, et al. (2007) IgG1 B cell receptor signaling is inhibited by CD22 and promotes the development of B cells whose survival is less dependent on Ig alpha/beta. *J Exp Med* 204:747–758.
48. Pelanda R, et al. (1997) Receptor editing in a transgenic mouse model: Site, efficiency, and role in B cell tolerance and antibody diversification. *Immunity* 7:765–775.
49. Lam KP, Rajewsky K (1999) B cell antigen receptor specificity and surface density together determine B-1 versus B-2 cell development. *J Exp Med* 190:471–477.
50. Kumar R, et al. (2015) Antibody repertoire diversification through VH gene replacement in mice cloned from an IgA plasma cell. *Proc Natl Acad Sci USA* 112: E450–E457.
51. Stadtfeld M, et al. (2010) Aberrant silencing of imprinted genes on chromosome 12qF1 in mouse induced pluripotent stem cells. *Nature* 465:175–181.
52. Shinkai Y, et al. (1992) RAG-2-deficient mice lack mature lymphocytes owing to inability to initiate V(D)J rearrangement. *Cell* 68:855–867.
53. Muramatsu M, et al. (2000) Class switch recombination and hypermutation require activation-induced cytidine deaminase (AID), a potential RNA editing enzyme. *Cell* 102:553–563.
54. Gallagher MP, Shrestha A, Magee JM, Wesemann DR (2014) Detection of true IgE-expressing mouse B lineage cells. *J Vis Exp*, 10.3791/52264.
55. Wesemann DR, et al. (2011) Immature B cells preferentially switch to IgE with increased direct Sμ to Sε recombination. *J Exp Med* 208:2733–2746.
56. Nakamura M, et al. (1996) High frequency class switching of an IgM+ B lymphoma clone CH12F3 to IgA+ cells. *Int Immunol* 8:193–201.
57. Guo C, et al. (2011) CTCF-binding elements mediate control of V(D)J recombination. *Nature* 477:424–430.
58. Schlissel MS, Baltimore D (1989) Activation of immunoglobulin kappa gene rearrangement correlates with induction of germline kappa gene transcription. *Cell* 58: 1001–1007.
59. Inlay MA, Tian H, Lin T, Xu Y (2004) Important roles for E protein binding sites within the immunoglobulin kappa chain intronic enhancer in activating Vkappa Jkappa rearrangement. *J Exp Med* 200:1205–1211.
60. Inlay MA, Lin T, Gao HH, Xu Y (2006) Critical roles of the immunoglobulin intronic enhancers in maintaining the sequential rearrangement of IgH and Igk loci. *J Exp Med* 203:1721–1732.

Supporting Information Appendix

Fig. S1

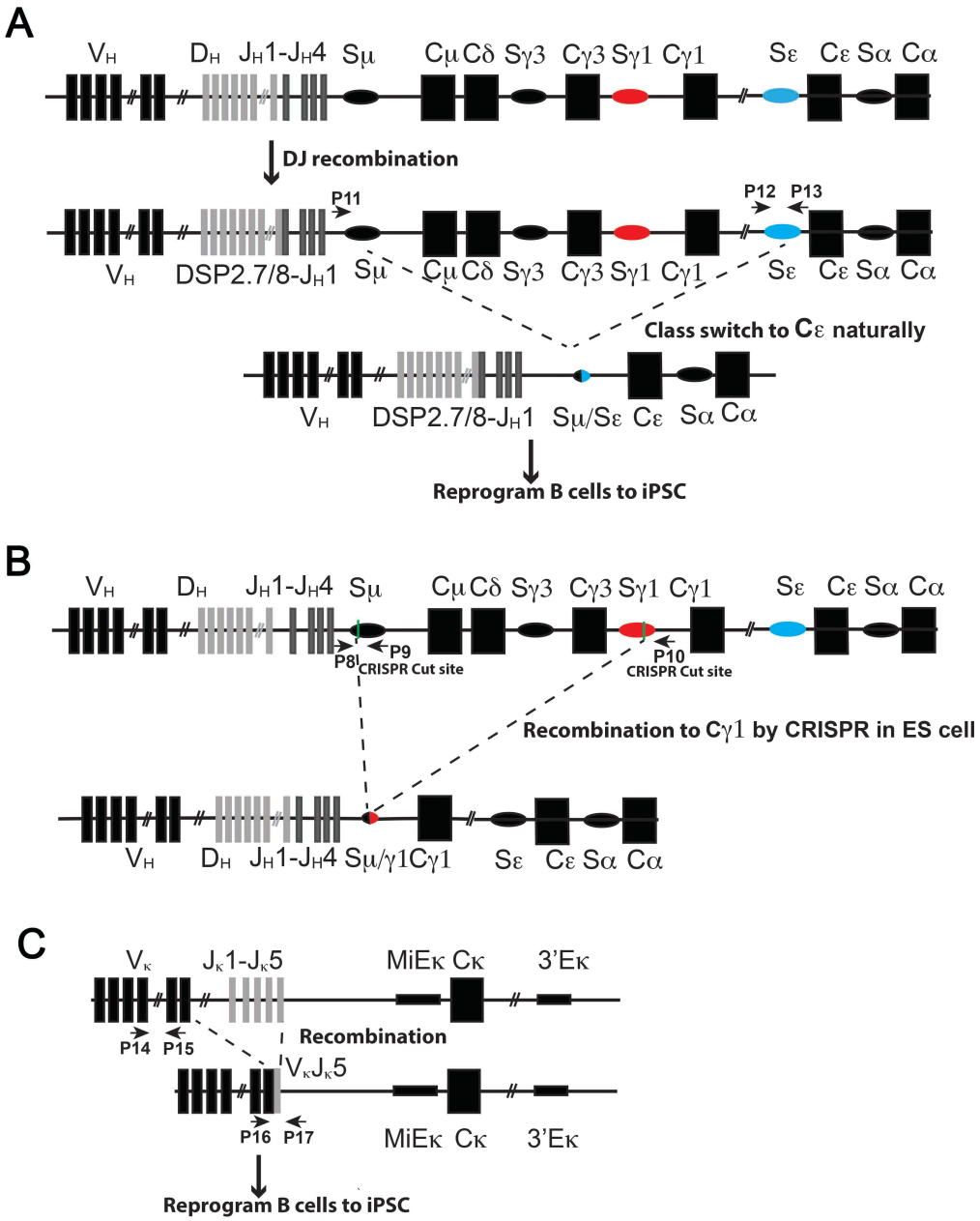

Fig. S1. Schematic diagram of the *Ighε* and *Ighγ*1 alleles and how they were generated. (*A*) Schematic diagram of the *Igh* locus in the original germline configuration (top) followed by a representation of pro-B cell D_HSP 2.7/8 to J_H1 recombination (middle). This non-productive allele had not undergone V_H to DJ_H recombination, but underwent *Igh* class switch

recombination to *Cε* as a mature activated B cell in vitro (bottom). The B cell carrying this allele was selected and reprogrammed to an induced pluripotent stem cell (iPSC) and the *Ighε* allele was isolated away from the other genes that allowed for the reprogramming to occur (*OKSM* and *rtTA*) through breeding. The *Igε* allele was then bred to homozygosity. Primer locations and primer names used for screening and genotyping are shown. Primer sequences can be found in Table S1. (*B*) Schematic diagram of the *Igh* locus in the original germline configuration (top) followed by a representation of the *Ighγ*1 allele after CRISPR-mediated recombination to *Cγ*1, which is essentially identical to what would be a natural CSR event (bottom). Germline mice were generated and the *Ighγ*1 allele was bred to homozygosity. Primer locations and primer names used for screening and genotyping are shown. (*C*) Schematic diagram of the *Igκ* locus in the original germline configuration (top) followed by a representation of an allele that had undergone *V*κ to *J*κ5 recombination (bottom). A mature B cell carrying the *VJ*κ5 allele was also isolated and reprogrammed as in panel (*A*). The *VJ*κ5 allele was then bred to homozygosity. Primer sequences can be found in Table S1.

Fig. S2

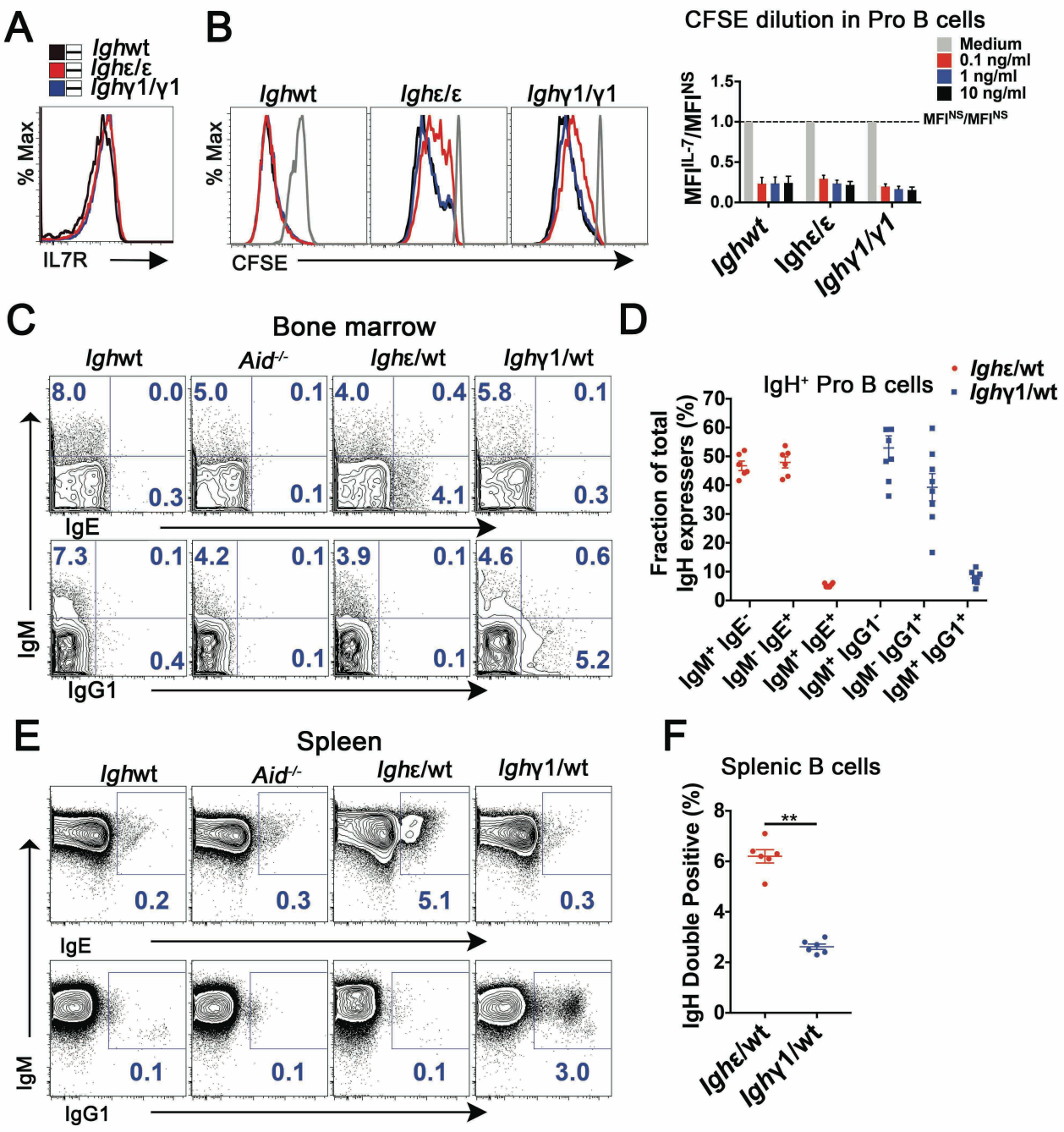

Fig. S2. IL-7 responses and allelic inclusion. (*A*) Flow cytometric histogram plot of live B220^{+} CD19^{+} BCR^{-} CD43^{+} pro-B cells from the indicated mice analyzed for surface IL-7R expression. Plot is representative of three experiments from at least 3 mice per genotype. (*B*) Flow cytometric histogram plots (left panel) and quantification (right panel) of live B220^{+}

$CD19^+$ BCR^- $CD43^+$ pro-B cells from the indicated mice analyzed for CFSE dilution after in vitro culture for 3 days with different dosage of IL-7 (*n*=5). Shown are MFI fold changes relative to the non-stimulated medium control (NS). One-way ANOVA followed by Tukey's post hoc test showed no significant change. Summary data are means ± SEM (*C* and *D*). Allelic inclusion in bone marrow B cells from *Igh*ε/*WT* and *Igh*γ1/*WT* mice. Representative FACS plots (*C*) and quantification graphs (*D*) showing intracellular Igμ, Igε, and Igγ1 heavy chains of bone marrow pro-B cells ($B220^{lo}$ $CD43^+$) of the indicated mice. Dot graph showing percentages of IgH single and double positive cells among total IgH expressing pro-B cells in *Igh*ε/*WT* (*n*=6) and *Igh*γ1/*WT* (*n*=8) mice. (*E* and *F*) Allelic inclusion in splenic B cells from *Igh*ε/*WT* and *Igh*γ1/*WT* mice. Representative FACS plots (*E*) and quantification plots (*F*) showing splenic B cells ($B220^+$ $CD19^+$) of the indicated mice. Cells were trypsinized to remove both membrane-bound and cytophilic IgH before fixation/permeabilization and staining for intracytoplasmic IgH. For FACS plots, *IghWT n*=2; $Aid^{-/-}$ *n*=2; *Igh*ε/*WT* *n*=6; *Igh*γ1/*WT n*=8. Dot graph showing percentages of IgH double positive splenic B cells from the indicated mice (*n*=6). ***P* < 0.01, two-tailed *t*-test. Summary data are mean values ± SEM.

Fig. S3

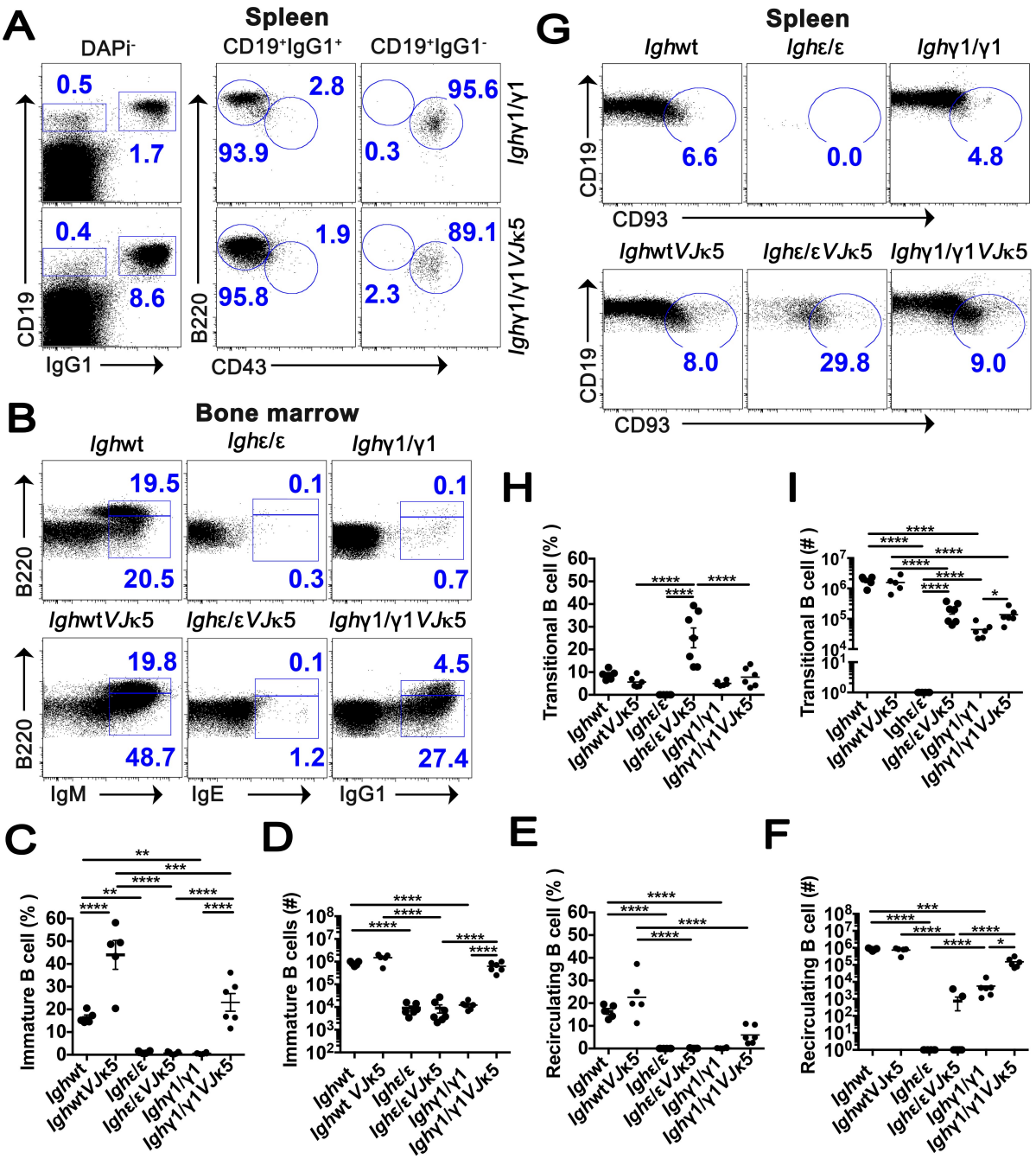

Fig. S3. Development and characteristics of B cells with and without pre-assembled *Igκ* (*VJκ*5). (*A*) FACS plots show splenic lymphocytes from the indicated mice. Numbers in the plots indicate percentages of cells within the live CD19$^+$ IgG1$^+$, CD19$^+$ IgG1$^-$, B220$^+$ CD43$^+$

and $B220^+$ $CD43^-$ gates as indicated (*n*=3-6). (*B*) FACS plots of live $B220^+$ $CD19^+$ bone marrow cells. Mature recirculating B cell ($B220^{hi}$ BCR^+) and immature B cell ($B220^{int}$ BCR^+) frequencies are indicated (*n*=5-6). (*C* and *D*) Dot graphs showing percentage (*C*) and absolute number (*D*) of immature B cells from indicated mice per femur (*n*=5-6). (*E* and *F*) Dot graphs showing percentage (*E*) and absolute number (*F*) of recirculating B cells from indicated mice per femur (*n*=5-6). (*G*) FACS plots of live transitional B cells ($CD19^+$ $B220^+$ $CD93^+$) from spleens of the indicated mice (*n*=5-6). (*H* and *I*) Dot graphs showing percentage (*H*) and absolute number (*I*) of transitional B cells of the indicated mice (*n*=5-6). $^*P < 0.05$, $^{**}P < 0.01$, $^{***}P < 0.001$, $^{****}P < 0.0001$, One-way ANOVA followed by Tukey's post hoc test. Data are mean values ± SEM.

Fig. S4

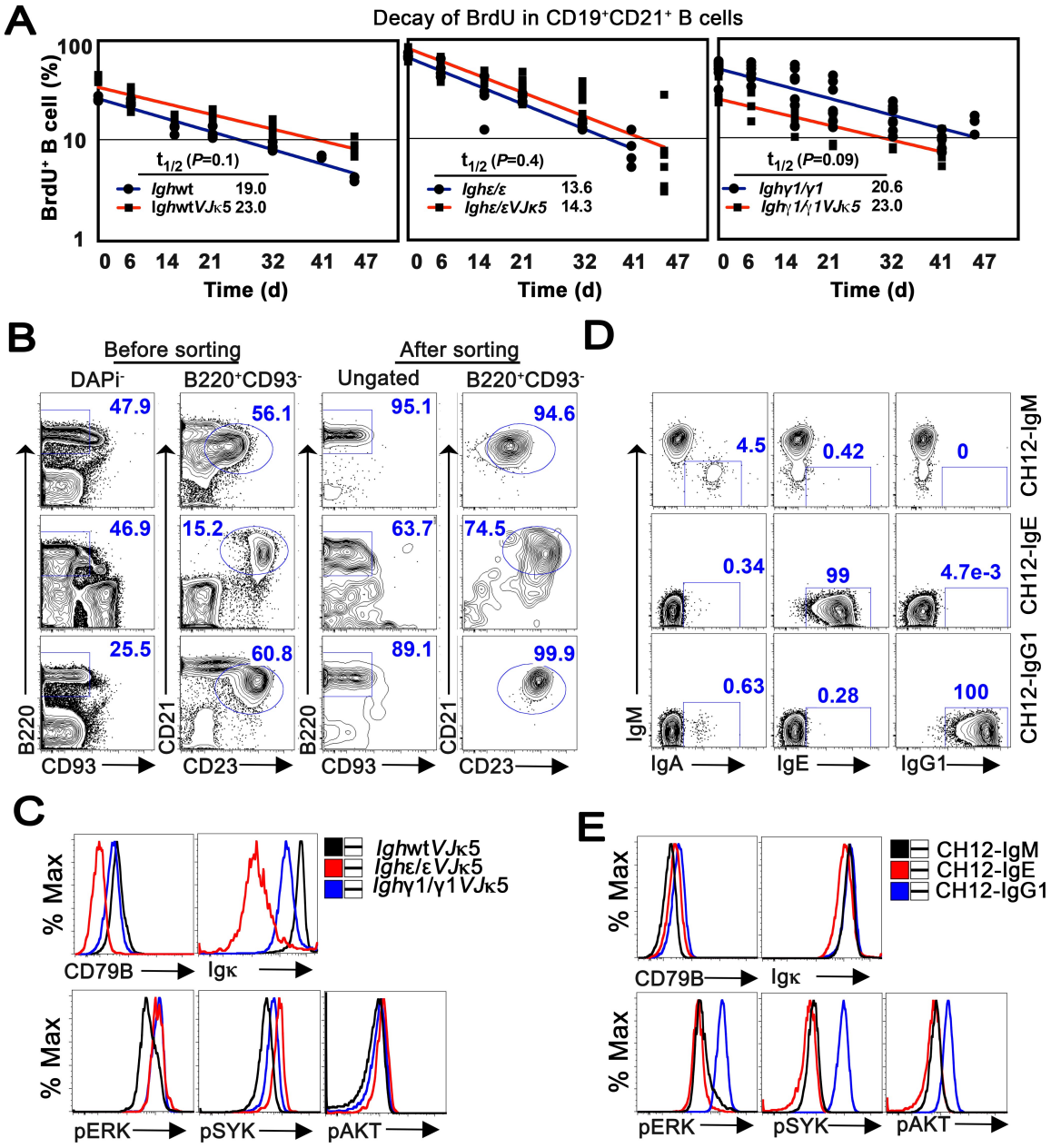

Fig. S4. Peripheral maintenance of B cells with the introduction of a pre-rearranged *Igκ* (*VJκ*5), sort purity for microarray experiments, and basal BCR related signaling analysis. (*A*) Half-life of peripheral B cells in the indicated mice. After a labeling period of 26 days, BrdU incorporation in mature peripheral blood B lymphocytes ($CD19^+$ $CD21^+$) was measured at the indicated time points (chase period from day 0 to day 47). Each dot represents an individual

mouse (*n*=4-8). Calculated decay curves and half-lives are shown. The *P* value was calculated by the two-tailed *t*-test. (*B*) Representative FACS plots showing CD23 and CD21 expression of splenic B cells from the indicated mice gated on live $B220^{+}$ $CD93^{-}$ lymphocytes before (left) and ungated after (right) sorting for follicular phenotype ($B220^{+}$ $CD93^{-}$ $CD21^{int}$ $CD23^{hi}$) B cells (*n*=3). Because CD23 staining intensity is higher in *Igh*ε/ε*VJ*κ5 and *Igh*γ*1*/γ*1VJ*κ5 mice, gating for $CD23^{+}$ cells is relative for each genotype. (*C*) BCR density (top panel) and intracellular staining of phospho (p)-ERK, p-SYK and p-AKT on resting splenic B cells from the indicated mice. Splenic B cells were negatively selected with anti-CD43 magnetic beads. MFI of CD79B (top left) and Igκ (top right) were measured by gating on live $CD19^{+}$ $B220^{+}$ B cells. MFI of p-ERK, p-SYK and p-AKT were measured by gating on intracellular $CD19^{+}$ $B220^{+}$ B cells (*n*=4). (*D*) FACs plots showing purity of CH12 cells, which express surface IgM, IgG1 and IgE from the endogenous productive *Igh* locus. (*E*) BCR density (top panel) and intracellular staining of p-ERK, p-SYK and p-AKT in CH12 cells. MFI of CD79B (top left) and Igκ (top right) were measured by gating on live BCR^{+} B cells. MFI of p-ERK, p-SYK and p-AKT were measured by gating on intracellular BCR^{+} B cells. Experiments were repeated at least three times.

Fig. S5

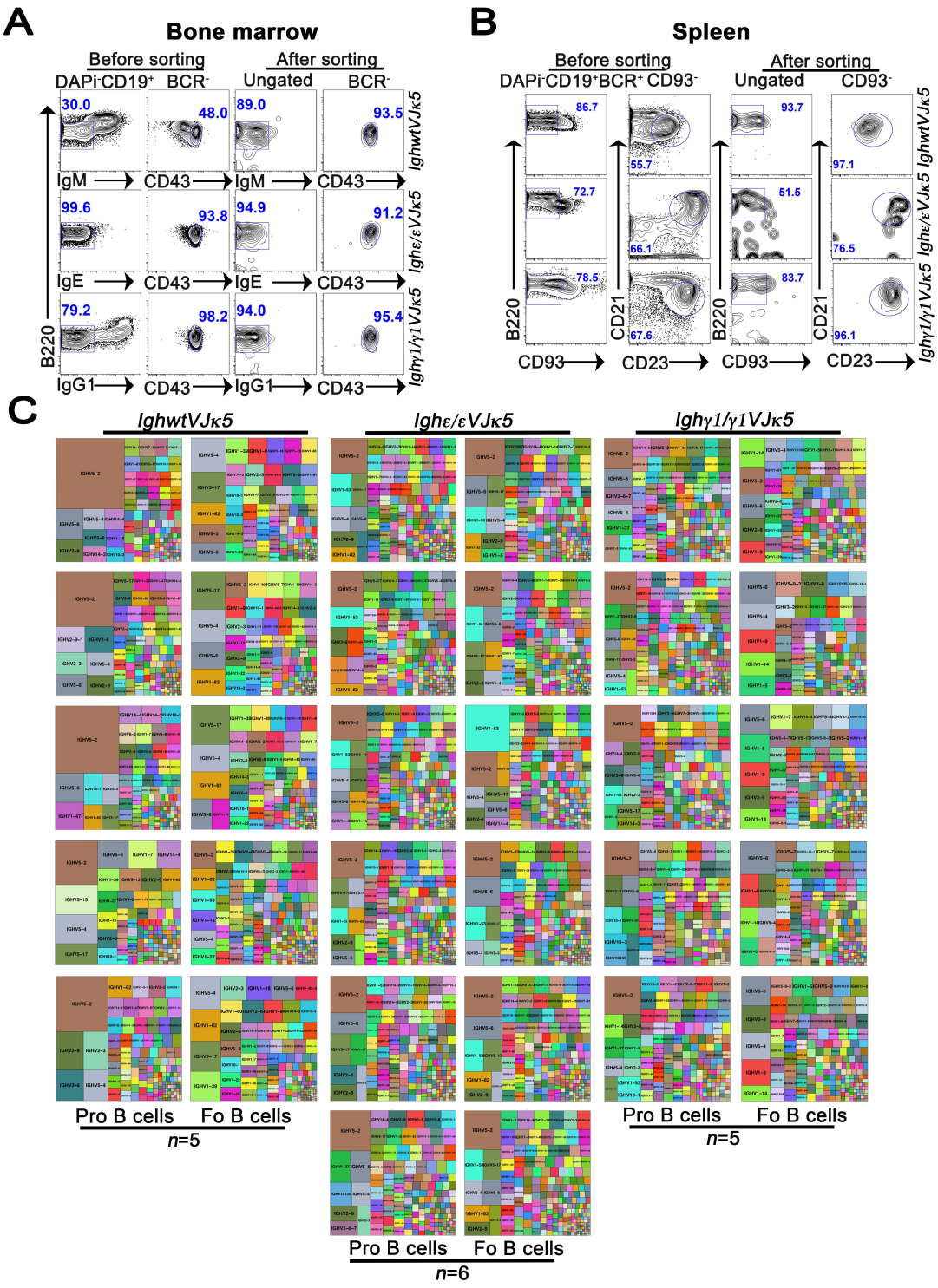

Fig. S5. Sort purity for deep sequencing, and V_H segment usage in pro-B and follicular B cells from *IghWTVJκ5*, *Ighε/εVJκ5* and *Ighγ1/γ1VJκ5* mice. (*A*) Representative FACS plots

showing B220^{+} CD43^{+} pro-B cells from the indicated mice gated on live CD19^{+} BCR^{-} before (left) and ungated after (right) sorting (*n*=5-6). (*B*) Representative FACS plots showing CD21^{int} CD23^{hi} follicular B cells gated on live CD19^{+} BCR^{+} CD93^{-} before (left) and ungated after (right) sorting in the indicated mice (*n*=5-6). Because *Igh*ε/ε*VJ*κ5 and *Igh*γ*1*/γ*1VJ*κ5 mice appear to express higher levels of CD23, the gating is relative within each mouse to identify CD23^{hi} CD21^{int} follicular B cells. (*C*) Treemaps of Ig repertoire sequencing data showing the distribution V_H gene segment usage for pro- and follicular (Fo) B cells in the indicated mice. Each map represents an individual mouse. Within a map, each colored box represents one V_H segment. The size of the box is directly proportional to the percentage of sequences harboring the V_H segment. The same V_H segment has the same color in all the treemaps.

Fig. S6

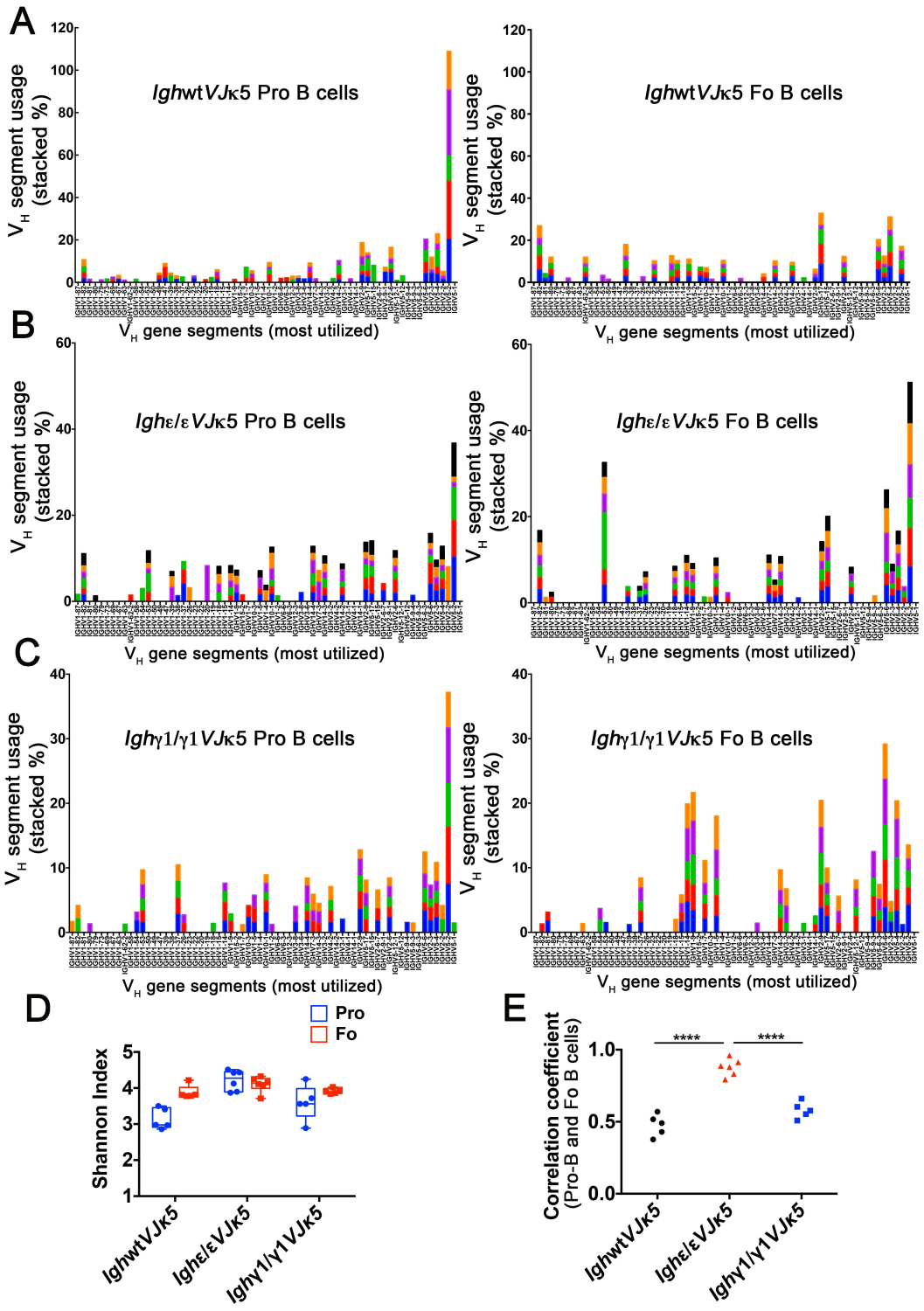

Fig. S6. *V_H* segment usage and diversity analysis in pro-B and follicular (Fo) B cells from *IghWTVJκ5*, *Ighε/εVJκ5* and *Ighγ1/γ1VJκ5* mice. (*A-C*) Stacked bar plots showing

cumulative percentage of sequences contributing to the most frequently utilized V_H gene segments for pro- and follicular (Fo) B cells in biologic repeats of *IghWTVJκ5* (*A*), *Ighε/εVJκ5* (*B*) and *Ighγ1/γ1VJκ5* (*C*) mice. Each color represents a different mouse. The V_H segments on the *x*-axis are arranged per natural geography, such that the most proximal V_H to the J_H region is on the right. (*D*) Box plot of Shannon diversity of V_H segments (with more than 5 sequences) for pro-B cells (blue) and follicular B cells (red) in the indicated mice. (*E*) Dot plot showing correlation coefficients of overall V_H segment usage correlations between pro- and follicular (Fo) B cells in *IghWTVJκ5* (black), *Ighε/εVJκ5* (red) and *Ighγ1/γ1VJκ5* (blue) mice. Each dot represents an individual mouse (n=5-6). The correlation coefficients were transformed using Fisher's r to z transformation and the *P*-value determined by one-way ANOVA followed by Tukey's post hoc test, ****$P < 0.0001$.

Fig. S7

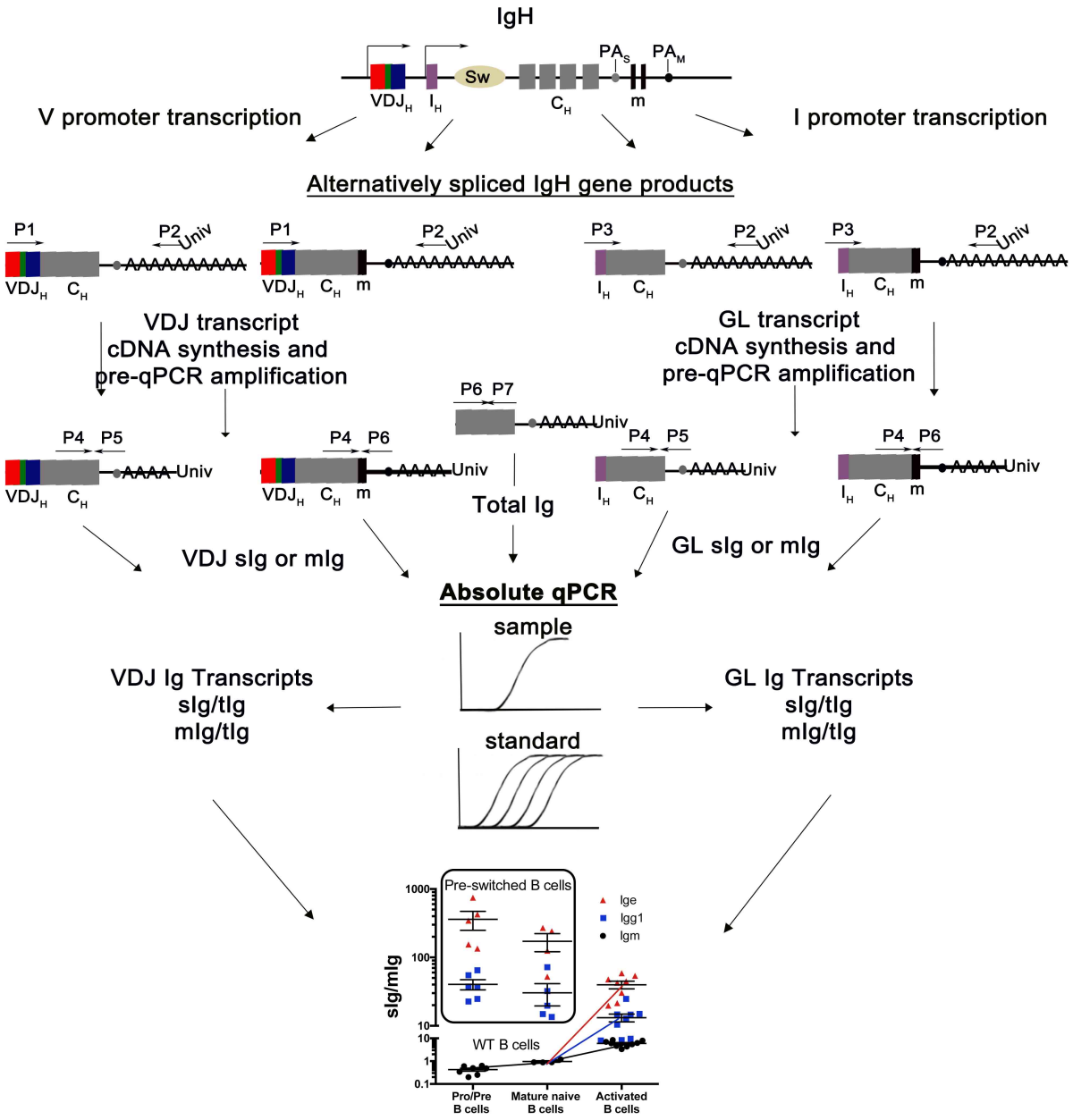

Fig. S7. Schematic diagram of the promoter-specific absolute quantitative PCR method used to measure sIg and mIg ratios. Representation of a productively assembled *Igh* locus, and the processed mRNA species resulting from both V_H promoter (productive) and I_H promoter (germline (GL)) transcripts. Primers used for enrichment of productive and GL transcripts, as well as the primers used for qPCR, are shown. Secreted Ig mRNA (sIg) and membrane Ig

mRNA (mIg) were measured by comparison to a known standard and divided by total Ig mRNA (tIg) measured the same way. The plot shown at the bottom is a modified re-representation of the data shown in Fig. 3 for schematic purposes. Primer sequences are found in Table S1.

Fig. S8

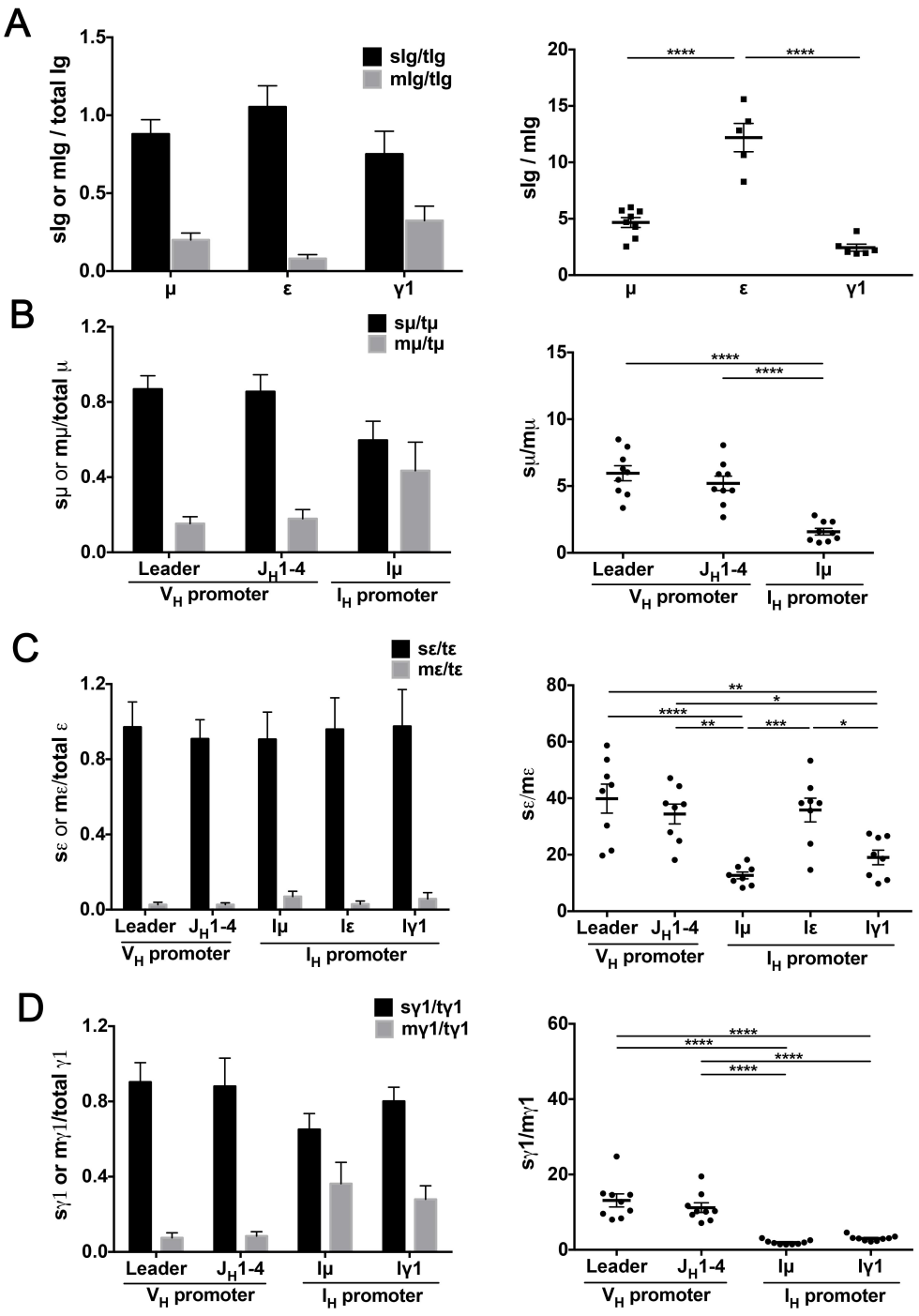

Fig. S8. Alternate promoter usage influences IgH mRNA alternative splice variant ratios. *(A)* Bar graph showing quantification of membrane (mIg) and secretory (sIg) Igμ, Igε and Igγ1

mRNA transcripts normalized to total Igμ, Igε or Igγ1 mRNAs, respectively from wild type magnetically purified $B220^+$ splenic B cells activated in vitro with anti-CD40 and IL-4 for 4 days. Amounts were measured in comparison to known standards by absolute quantitative PCR using cDNA as a template (*n*=4-5). The dot graph to the right shows the data represented as sIg/mIg ratios. *(B-D)* Bar graphs showing quantification of membrane (mIg) and secretory (sIg) IgH mRNA as in *(A),* by using pre-amplified templates enriched for V_H promoter (productive) transcripts or I_H promoter (GL) transcripts as a template (*n*=9). Productive transcripts were enriched with 16 cycles of PCR using either a leader sequence primer or a mixture of primers recognizing all four J_H sequences as forward primers as indicated. GL sequences were enriched with a primer specific for non-coding I_H exons, which are driven by the I_H region promoter, as forward primer. The enrichment steps for both V_H and I_H transcripts share the same universal reverse primer. Measurements for Igμ *(B), Igε (C) and Igγ1 (D)* are shown in the context of productive transcripts as well as several possible I_H-C_H combinations that can result from *Igh* recombination events. Dot graphs to the right show the data represented as sIg/mIg ratios. **P* < 0.05, ***P* < 0.01, ****P* < 0.001, *****P* < 0.0001, one-way ANOAVA followed by Tukey's post hoc test. Data are mean values ± SEM.

Fig. S9

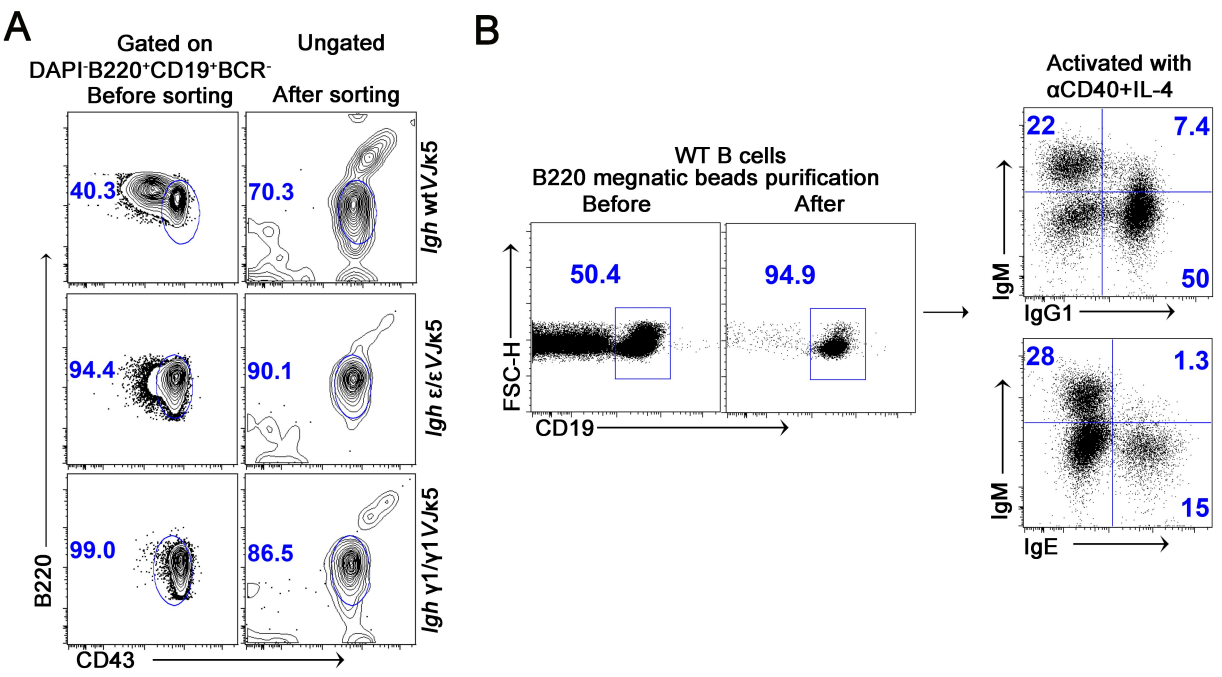

Fig. S9. B cell purification and analysis for qPCR. (*A*) Representative FACS plots showing CD43$^+$ BM cells from the indicated mice gated on live B220$^+$ CD19$^+$ BCR$^-$ before (left) and ungated after (right) sorting for pro-B cells. (*B*) Representative FACS plots showing magnetic isolation of splenic B cells with B220 beads before and after purification (left) and intracellular IgM, IgG1, and IgE staining of the activated wild type B cells (right). Results are representative of at least 4 experiments.

Fig. S10

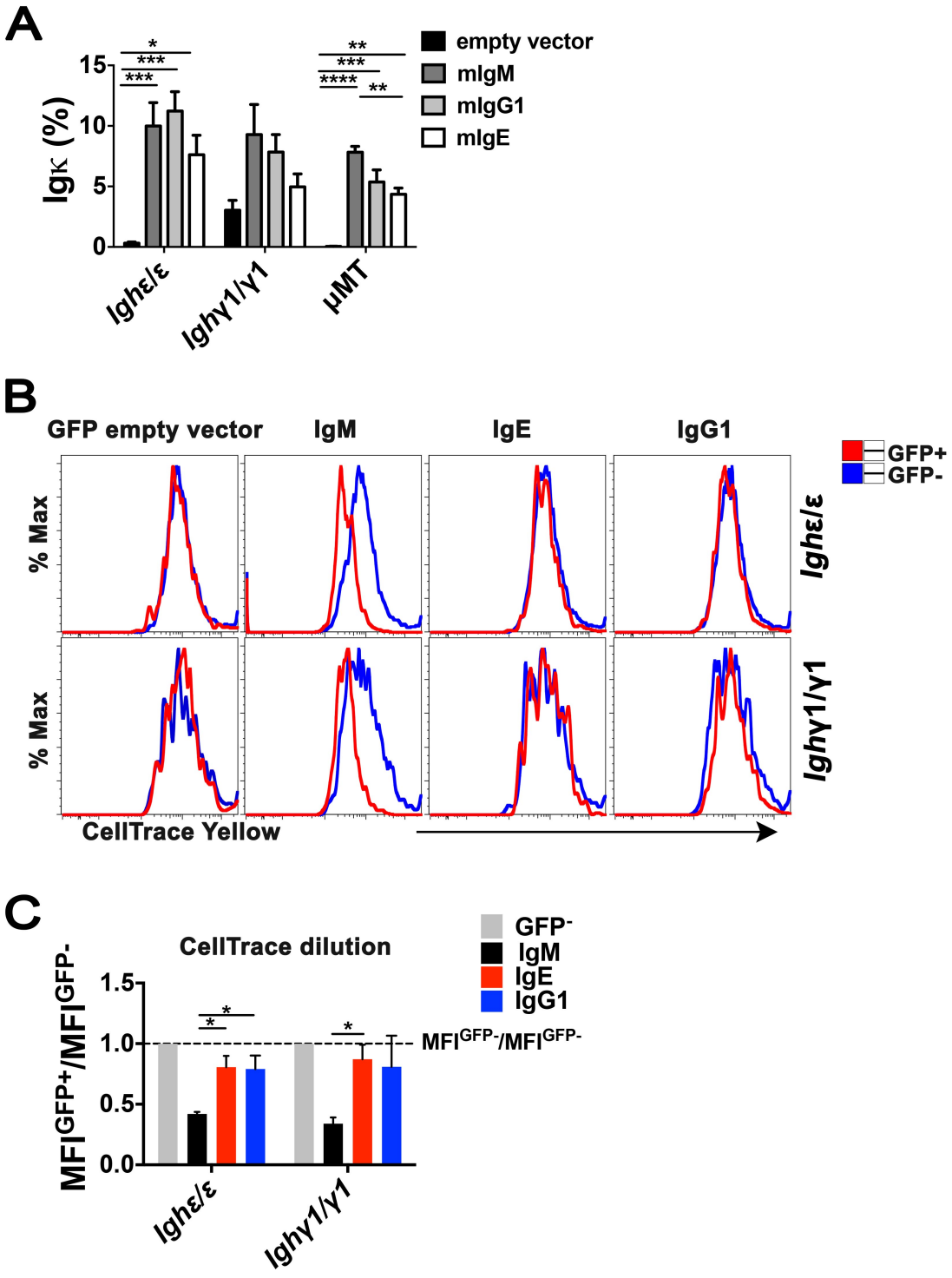

Fig. S10. Retrovirus transduction in bone marrow B cells. (*A*) Bar graph showing percentage of surface Igκ$^+$ on total live CD19$^+$ GFP$^+$ B cells from *Ighε/ε, Ighγ1/γ1* and μMT mice after

retroviral transduction (*n*=4-6). *$P < 0.05$, **$P < 0.01$, ***$P < 0.001$, ****$P < 0.0001$, one-way ANOVA followed by Tukey's post hoc test. Data are mean values ± SEM. (*B*) Proliferation of bone marrow B cells from *Igh*ε/ε and *Igh*γ1/γ1 mice transduced with retrovirus carrying mIgM, mIgE and mIgG1. GFP^+ and GFP^- B cells are gated from live $CD19^+$ cells. (*C*) Quantification of live $CD19^+$ B cells from panel (*B*) analyzed for CellTrace dilution after retrovirus transduction for 3 days (*n*=3). Shown are MFI fold changes in GFP^+ population relative to the GFP^- population. *$P < 0.05$, one sample *t* test. Summary data are means ± SEM.

Table S1

Reverse transcription		
UNV-8N-oligodT18		AAGCAGUGGUAUCAACGCAGAGNNNNN-NTTTTTTTTTTTTTTTTVN
VH leader Fw	P1	GAGGTGCAGCTGCAGGAGTCTGG
JH1-4 Fw (pool)		GAACAGAGGCAGAACAGAGACT
		TTTGACTACTGGGGCCAAGG
		AGGGACTCTGGTCACTGTCT
		AGGAACCTCAGTCACCGTCT
UNV Rv	P2	AAGCAGTGGTATCAACGCAGAG
Iε Fw	P3	GAGATTCACAACGCCTGG
Iμ2 Fw		CTCGGTGGCTTTGAAGGAAC
Iγ1 Fw		TCGAGAAGCCTGAGGAATGT
sμ Fw and mμ Fw	P4	TGGAACTCCGGAGAGACCTA
sγ1 Fw		TGCACAACCACCATACTGAGA
mγ1 Fw		CAATGTGCAGAAGAGCAACTGG
sε Fw		CTAGAGGTCGCCAAGACACTC
mε Fw		CGCCTAGAGGTCGCCAAGAC
sμ Rv	P5	GTGCCGCCTGTGTCAGACA
mμ Rv		TTCCTCCTCAGCATTCACCT
sγ1 Rv		GGGTGGAGGTAGGTGTCAGA
mγ1 Rv		CTCAGCACAGGTCTCGTCCA
sε Rv		AGGGACGGAGGGAGGTGTTA
mε Rv		AGCTCACACTGAGCAGGAAC
tμ Fw	P6	CTCGTGAGCAACTGAACCTGA
tγ1 Fw		AACAGCACTTTCCGCTCAGT
tε Fw		CGAGGACAAACGCACACTCA
tμ Rv	P7	GCAAGAGTTGCCCTCTCTGAA
tγ1 Rv		AAAGCTGCACTGTTGACCCT
tε Rv		GAGATCAGTTTGCCATCCCCC
CRISPR		
Cas9Guide Mu Fw 1		GTAAACTGTTTCTGCTTAAG
Cas9Guide Mu Rv 1		CTTAAGCAGAAACAGTTTAC
Cas9Guide Gamma1 Fw 2		GATATCACCTACTCCATGTAGAGAGTCG
Cas9Guide Gamma1 Rv 2		CGACTCTCTACATGGAGTAGGTGATATC
Genotyping		
Cas9 mu Fw	P8	CAGGCACCGCAAATGGTAAG
Cas9 mu Rv	P9	GAGACAGCATCAGTACCTCAACT
Cas9 Cgamma1 Rv	P10	GGAAGGTGTGCACACCGCTGGAC
Smu 320-23	P11	GCTGGCTTAACCGAGATGAG
Seps WT	P12	GGGGCTAAGAGGAGCTGAGT
Seps 320-23	P13	CCAGTTTACCTCAGCCCAGA
Jκ WT Fw	P14	TGGAGAATGAATGCCAGTGT
Jκ WT 171 Rv	P15	CCCCTTCCGAACGTGTA
$V\kappa_o$ Fw	P16	GGCTGCAGSTTCAGTGGCAGTGGRTCWGGRAC
Jκ5 Rv	P17	ATGCGACGTCAACTGATAATGAGCCCTCTCC

VDJ rearrangement	
VHJ558v.2	ARGCCTGGGRCTTCAGTGAAG
VH7183v.2	GTGGAGTCTGGGGGAGGCTTA
JH4e	AGGCTCTGAGATCCCTAGACAG
DLG5 exon6 Forward	AAGTCTCAGGCTGGCCATTA
DLG5 exon6 Reverse	TTTACCACCCCTGACACACA
VJκ rearrangement PCR	
Vkappa forward	GGCTGCAGSTTCAGTGGCAGTGGRTCWGGRAC
Mar35	AACACTGGA TAAAGCAGTTTATGCCCTTTC
Igk intron Fw	ATGACCCAGAGGATGAAAC
VJκ rearrangement qPCR	
Vkappa, forward primer	GGCTGCAGSTTCAGTGGCAGTGGRTCWGGRAC
Jk1-2 Rv	GACAACGGAAGAAAGAGACTTTGGA
Intronic b-actin	
ibactin Fw	GAGGCTCTTTTCCAGCCTTC
ibactin Rv	TCCATACCTAAGAGAAGAGTGACAGA
Deep Sequencing	
Reverse transcription	
U3' Cmu outer	AGGGGGCUCUCGCAGGAGACGAGG
U3' Cg1 outer	GGAAGGUGUGCACACCGCUGGAC
U3'Cep outer	CACUUGGCUGGUGGUGACCUUG
IgH Barcode-UMI-8N-leader Fw	AAGCAGTGGTATCAACGCAGAGNNNNNN-NNGAGGTGCAGCTGCAGGAGTCTGG
Preaplification-CS1 Fw	TACACTGACGACATGGTTCTACA
3'Cep inner Rv	GGCAGCCCAGGGTCATGGAAG
3'Cep inner Rv	GCTCAGGGAAATAGCCCTTGAC
First round IgH PCR	
CS1-UNV Fw	TACACTGACGACATGGTTCTACAAAGCAGTG-GTATCAACG
I7-3'Cmu inner Rv	TACGGTAGCAGAGACTTGGTCTAGTAGGGGG-AAGACATTTGGGAAGGAC
I7-3'Cep inner Rv	TACGGTAGCAGAGACTTGGTCTGCTGGCAGC-CCAGGGTCATGGAAG
I7-3'Cg1 inner Rv	TACGGTAGCAGAGACTTGGTCTTCAGCTCAG-GGAAATAGCCCTTGAC
Second round PCR	
P5-CS1	AATGATACGGCGACCACCGAGATCTACACTGA-CGACATGGTTCTACA
P7-index-CS2	CAAGCAGAAGACGGCATACGAGAT[sample-barcode]TACGGTAGCAGAGACTTGGTCT

Table S1. Primer names and sequences

SI Appendix Materials and Methods

Mice

The Children's Hospital Boston Animal Care and Use Committee (IACUC) and the Warren Alpert Building IACUC approved all experiments. All mice were maintained in a specific pathogen-free (SPF) environment and housed in clear cages in groups of up to five animals per cage with constant temperature and humidity and a 12 h/12 h light/dark cycle. All animals had access to water at all times and were fed with regular chow. Doxycycline-inducible reprogrammable mice used in these experiments have been described previously (1, 2) and were a gift from Konrad Hochedlinger (Massachusetts General Hospital, Boston, MA). Splenic B cells from reprogrammable mice were isolated and CSR to IgG1 and IgE was induced as described previously (2). Mice germline for the switched *Cε* allele were bred to homozygosity while the reprogramming factor (*OKSM*) and the *rtTA* gene cassettes were bred out and were designated *Igh*ε/ε mice. A pre-assembled *VJ*κ5 allele was also isolated via this method. The polyclonal Ig heavy chain allele pre-switched to *C*γ1 was generated by electroporation of TC1 ES cells with CRISPR constructs targeting both *S*μ and *S*γ1 regions to delete intervening sequence (Fig. S1). Targeted clones were screened and sequenced to confirm correct targeting as outlined (Fig. S1). Homozygous mice for *Igh*γ1 allele were generated and here denoted by *Igh*γ1/γ1 mice. The *Igh*γ*/*γ*1*, *IghWT*, *Igh*ε*/*ε*,* and *VJ*κ5 variants were all maintained on a mixed 129.B6 background. The μMT mice (*B6.129S2-Ighm^{tm1Cgn}/J)*, *Pten*$^{c/c}$ (*B6.129S4-Pten^{tm1Hwu}/J*) mice and *Cd19*cre (*B6.129P2(C)-Cd19tm1(cre)Cgn/J)* mice were purchased from The Jackson Laboratory. The *Rag2*$^{-/-}$ mice were described previously (3), were provided by Dr. Frederick Alt (Boston Children's Hospital). Tasuku Honjo provided the *Aid*$^{-/-}$ mice (4). Unless otherwise noted, all mice were housed at the Boston Children's

Hospital animal facility under SPF conditions. AID-cre-ERT2 Rosa26-loxp-EYFP mice were housed in the Warren Alpert Building under SPF conditions.

Cell Isolation and Flow Cytometry

Bone marrow cells were flushed from femurs and tibias with ice cold staining buffer (PBS supplemented with 2% FBS). Splenic cell suspensions were obtained by gently teasing spleens onto a 70 μm cell strainer. Erythrocytes were depleted using red blood cell lysis buffer (Sigma). Cells were counted using a hemocytometer with exclusion of dead cells with trypan blue dye. Cells were stained with fluorophore or biotin conjugated antibodies against mouse B220 (RA3-6B2), CD19 (6D5), CD23 (B3B4), IgM (RMM-1), IgE (RME-1), IgG1 (RMG1-1), CD79b (HM79-12), GL7 (GL7), CD38 (90) from Biolegend; CD19 (1D3), CD43 (S7), IgE (R35-72), IgG1 (A85-1), Igκ light chain (187.1) p-ERK1/2 (T202/Y204), p-SYK (Y348) and p-AKT (S473) from BD Biosciences; CD21 (8D9), CD93 (AA4.1), from eBiosciences; IgM (1B4B1) from SoutherBiotech. Intracytoplasmic IgE, IgG1, IgM staining and flow cytometry were performed as described (5, 6) where indicated. Briefly, cells were incubated in 0.05% trypsin (Gibco) for 1-2 min in PBS at room temperature, followed by fixation in 1% buffered paraformaldehyde (Electron Microscopy Sciences) for 20 min at room temperature. Cells were then permeabilized with permeabilization buffer (BD Bioscience) or 0.1% saponin (Sigma-Aldrich) for 20 min on ice, washed twice, and stained for intracellular antigens at room temperature in the same buffer. For non-fixed cells, DAPI was added at 2.5 μg/ml for dead cell exclusion. For phospho-epitope staining, splenic cells were negatively selected by anti-CD43 beads (Miltenyi Biotech). Cells were fixed in 2% buffered paraformaldehyde for 20 min at room temperature, then permeabilized with 100% Methanol on ice for 2 hours. After twice wash, cells were stained with p-ERK1/2, p-SYK and p-AKT. For

cell proliferation experiment, bone marrow cells from *IghWT*, *Igh*ε/ε and *Igh*γ1/γ1 mice were isolated by B220 positive selection via magnetic columns (Miltenyi Biotech) according to manufacture instructions. The purified cells were stained with CellTrace^{TM} CFSE, then plated in 24-well plate (1X10^5/well) and cultured in the presence of IL-7 (10 ng/mL, 1 ng/mL and 0.1 ng/mL) or absence of IL-7 for 3 days. Cells were analyzed by FACS. Flow cytometry was performed on FACSCanto II flow cytometer (BD Biosciences). The cell sorting was performed on FACSAria II flow cytometer (BD Biosciences). Data analysis was performed at FlowJo software (v9.9.4).

Generation of CH12-IgG1 and CH12-IgE Cell Lines and Overexpression of mIgH in Pro-B Cells

CH12 cells were activated in culture with anti-CD40 plus IL-4 for 4 days and IgE and IgG1 expressing CH12 cells were serially sorted for isotype purity. The cDNAs for mIgM, mIgG1 and mIgE were prepared from the CH12 B cell line (mIgM) or CH12-derived CH12-IgG1 and CH12-IgE cell lines and cloned into the pMIG vector (Addgene). To pack the retrovirus, the pMIG constructs were transiently transfected into 293T cells with pCL-eco using lipofectamine. Forty-four hours after transfection, viral supernatants were harvested, filtered, frozen, and aliquots were tested on NIH 3T3 cells. Bone marrow cells from *Igh*ε/ε, *Igh*γ1/γ1 and μMT mice were cultured in the presence of IL-7 (20 ng/mL). After 2-3 days, cultured bone marrow cells were infected with GFP or mIgH–encoding retroviruses. After 2 additional days, culture medium was removed and cells were cultured in the presence of BAFF (20 ng/mL) and IL-4 (10 ng/mL) for 3 days. Kappa chain rearrangement was analyzed by flow cytometry. For cell proliferation experiment, bone marrow cells from *Igh*ε/ε and *Igh*γ1/γ1 mice were cultured in the presence of IL-7 (20 ng/mL) for 2 days. The cells were stained with

CellTrace™ yellow proliferation dye (Thermo Fisher Scientific) and then infected with GFP or mIgH–encoding retroviruses. Cells were cultured with IL-7 (20 ng/mL) for additional 3 days before cell proliferation was analyzed flow cytometrically.

DNA Isolation and Ig Rearrangement Analysis

Cells were lysed in proteinase K lysis buffer (100 mM Tris·HCl pH 8.0, 5 mM EDTA, 0.2% SDS and 200 mM NaCl, 200 μg/mL proteinase K) followed by genomic DNA precipitation with 50% isopropanol. After washing with 70% ethanol, DNA was resuspended in T-low-E buffer (10 mM Tris pH 8.0, 0.1 mM EDTA). Threefold serial dilutions of genomic DNA (approximately 100 ng, 30 ng, and 10 ng) were used to perform PCR to analyze Ig heavy chain VDJ_H and Ig light chain $V\kappa$-$J\kappa$ rearrangements. Two main V_H families were analyzed (7183 and J558) using primers described previously (7). For a loading control, primers flanking exon 6 of the *Dlg5* gene were used. (Table S1). $V\kappa$–$J\kappa$ rearrangement products were PCR amplified using a degenerate $V\kappa$ and the Mar35 primers described previously (8). Primers in the *Igκ* intron were used as a loading control (Table S1). $V\kappa$–$J\kappa 1$ rearrangement was also determined by quantitative PCR assay using the degenerate $V\kappa$ forward primer and a reverse primer complementary to sequences downstream of $J\kappa 1$ (Jκ1-2R) as described previously (9, 10). Rearrangement levels measured by qPCR were normalized to the levels of a *β-actin* DNA.

Isolation and Measurement of Membrane Secretory IgH mRNA

Cell mRNA was isolated using Dynabeads® mRNA DIRECT™ Micro Purification Kit (ambion/Life technologies), followed by DNA elimination with gDNA wipeout (Qiagen). cDNA was obtained using Superscript III reverse transcription system (Invitrogen) using anchored

Oligo $(dT)_{20}$ primers (Invitrogen). When V_H and I_H promoter-driven transcripts were analyzed, the reverse transcription (RT) step was performed with anchored oligo dT coupled to an universal sequence (Table S1), followed by a PCR step to amplify either V_H or I_H promoter-driven transcripts. For V_H promoter transcripts, the V_H segment leader sequence (V_H leader Fw) was used as a forward primer. A mixture of forward primers against all four J_H regions (J_H1-4 Fw) was also used (Table S1). For I_H promoter transcript amplification, Primers complementary to Iμ, Iε, or Iγ1 (Iμ2 Fw, Iε Fw or Iγ1 Fw) were utilized as forward primers; the reverse primer (UNV Rv) was the universal sequence that was appended to the poly T primer on the RT step. A total of 16 or 25 cycles were used to amplify either V_H or I_H containing transcripts. PCR conditions were as follows: pre-amplification to amplify either V_H or I_H containing transcripts with only forward primer, 94°C, 2 minutes, 3 cycles at 94°C for 10 seconds, 58°C for 30 seconds, 68°C for 3 minutes, after 3 cycles, 68°C for 7 minutes to end the reaction. Column purification (Qiagen) was used to purify the pre-amplification PCR products, followed by PCR with forward primer and reverse primer. PCR amplification, 94°C, 2 minutes, 16 or 25 cycles at 94°C for 10 seconds, 58°C for 30 seconds, 68°C for 3 minutes, after 16 or 25 cycles, 68°C for 7minutes to end the reaction. PCR products were diluted at least 100 times and analyzed by quantitative PCR. Quantitative PCR using FastStart Universal SYBR green system (Roche) was deployed to analyze membrane or secretory IgH levels in total cDNA or amplified DNA enriched for either V_H or I_H promoter-driven transcripts. Levels were normalized by total μ, ε or γ1 transcripts using primers located in the shared constant exon. The following primers set were used: mμ, sμ and tμ; mε, sε and tε; mγ1, sγ1 and tγ1 (Table S1). Absolute quantification was determined by standard curves with linearized pGEM plasmids expressing mIgM, sIgM, mIgE, sIgE, mIgG1 or sIgG1 genes cloned from CH12 cells (for IgM), as well as CH12 isolated after in vitro CSR to IgE (CH12-

IgE for IgE) and IgG1 (CH12-IgG1 for IgG1). Absolute amount of the standard DNA was determined by Tapestation (Agilent 2200 TapeStation).

BrdU Labeling

For BrDU experiments, 0.8 mg/ml BrdU (Sigma-Aldrich) was given in the drinking water for 26 days then provided normal water. Peripheral B cells were harvested from blood at various time points and stained with CD19 and CD21. The BrdU flow kit (BD Biosciences) was used for BrdU detection.

Deep Sequencing

Pro-B cells ($DAPi^-$ $B220^+$ $CD19^+$ BCR^- $CD43^+$) and follicular B cells ($DAPi^-$ $CD19^+$ BCR^+ $CD93^-$ $CD23^{hi}$ $CD21^{int}$) were sorted from *IghWTVJκ5*, *Ighγ1/γ1VJκ5* and *Ighε/εVJκ5* mice. RNA was reverse-transcribed into cDNA using immunoglobulin heavy chain constant region specific primers. Reverse transcriptase was heat inactivated and residual primers removed using Uracyl DNA glycosylase. The glycosylase was then heat inactivated. IgH cDNA was provided with a unique molecular identifier (UMI) during for one round of second strand DNA synthesis at 98°C for 1 min, 58°C for 1 min, 72°C for 10 min with Phusion DNA polymerase (Thermo Fisher Scientific). The residual UMI-containing primers were removed by purifying with RNAClean XP beads. For samples from *Ighγ*1/γ1*VJκ*5 and *Ighε/εVJκ*5 mice, 9 cycles pre-amplification was used to enrich the products before first round PCR, which was performed at 98°C for 30 sec, followed by 9 cycles of 98°C for 10 sec, 55°C for 30 sec, 72°C for 30 sec and final incubation at 72°C for 5 min. Qiaquick PCR purification kit was used to purify the pre-amplification products. Double stranded cDNAs, or pre-amplification products were amplified by a first round of PCR, which added 5' and 3' adaptors using 98°C for 30 sec,

followed by 25 cycles of 98°C for 10 sec, 60°C for 30 sec, 72°C for 30 sec and final incubation at 72°C for 5 min, followed by Qiaquick PCR purification. Second round PCR added Illumina linkers (P5 and P7) and sample barcodes to IgH mRNA using 98°C for 30 sec, followed by 17 cycles of 98°C for 10 sec, 60°C for 30 sec, 72°C for 30 sec and final incubation at 72°C for 5 min. All the primers used for the deep sequencing are listed in Table S1.Products were quantified on a Qubit fluorimeter, run on a fragment analyzer with amplicon regions and expected sizes confirmed. Samples were then pooled in equal amounts according to product concentration. The pooled products were then size selected on an agarose gel and purified by gel extraction. Purified, size-selected products were run on an Agilent Bioanalyzer to confirm appropriate profile and determination of average size. The final pools were quantitated using Qubit. 5 nM dilutions were further quantitated by qPCR on a BioRad CFX Connect Real-Time System and pooled evenly. The pool was denatured and spiked with 15% non-indexed PhiX control library provided by Illumina and loaded onto the MiSeq V2 Nano flowcell at a concentration of 7 pM for cluster formation and sequencing. The PhiX control library provides a balanced genome for calculation of matrix, phasing and prephasing, which are essential for accurate basecalling. The libraries were sequenced from both ends of the molecules to a total read length of 250 nt from each end.

Sequencing Data Analysis

The sequences obtained from Illumina MiSeq deep sequencing (nano-run) were run through the standalone IgBlast software (version 1.4.0) to identify the V_H segment using reference sequences from IMGT. PCR repeats were filtered using unique molecular identifies (UMIs) applied during cDNA synthesis. Sequences with the same V_H and the same UMI were considered PCR repeats of the same mRNA. Only forward reads (R1) are used, as the

quality of R2 sequences was poor leading to low merge efficiency. Also, the CDR3 regions predicted were not reliable due to low quality intermittent nucleotides. By using only the UMIs and the V_H, we risk loosing some unique sequences attached to the same UMI at the cost of excluding all PCR repeats. The frequency of usage of each V_H was calculated and compared for *IghWTVJ*κ5, *Igh*ε/ε*VJ*κ5, and *Igh*γ1/γ1*VJ*κ5 mice. All preprocessing and analysis was done using Bioconductor package v 3.4 (R version 3.3.1).

Data Availability

The raw sequence data for this study are accessible at the NCBI Sequence Read Archive (SRA) under BioProject accession number PRJNA394007 with BioSample accession numbers SAMN07347175 - SAMN07347206.

SI Appendix References

1. Stadtfeld M*, et al.* (2010) Aberrant silencing of imprinted genes on chromosome 12qF1 in mouse induced pluripotent stem cells. *Nature* 465(7295):175-181.
2. Wesemann DR*, et al.* (2012) Reprogramming IgH isotype-switched B cells to functional-grade induced pluripotent stem cells. *Proceedings of the National Academy of Sciences of the United States of America* 109(34):13745-13750.
3. Shinkai Y*, et al.* (1992) RAG-2-deficient mice lack mature lymphocytes owing to inability to initiate V(D)J rearrangement. *Cell* 68(5):855-867.
4. Muramatsu M*, et al.* (2000) Class switch recombination and hypermutation require activation-induced cytidine deaminase (AID), a potential RNA editing enzyme. *Cell* 102(5):553-563.
5. Gallagher MP, Shrestha A, Magee JM, & Wesemann DR (2014) Detection of true IgE-expressing mouse B lineage cells. *J Vis Exp* (94).

6. Wesemann DR*, et al.* (2011) Immature B cells preferentially switch to IgE with increased direct Smu to Sepsilon recombination. *The Journal of experimental medicine* 208(13):2733-2746.

7. Guo C*, et al.* (2011) CTCF-binding elements mediate control of V(D)J recombination. *Nature* 477(7365):424-430.

8. Schlissel MS & Baltimore D (1989) Activation of immunoglobulin kappa gene rearrangement correlates with induction of germline kappa gene transcription. *Cell* 58(5):1001-1007.

9. Inlay MA, Tian H, Lin T, & Xu Y (2004) Important roles for E protein binding sites within the immunoglobulin kappa chain intronic enhancer in activating Vkappa Jkappa rearrangement. *The Journal of experimental medicine* 200(9):1205-1211.

10. Inlay MA, Lin T, Gao HH, & Xu Y (2006) Critical roles of the immunoglobulin intronic enhancers in maintaining the sequential rearrangement of IgH and Igk loci. *The Journal of experimental medicine* 203(7):1721-1732.